약학박사학위논문

급성 감염 상황에서 단구 유래 수지상 세포가 기억 CD8 T 세포 분화에 미치는 영향에 대한 연구

Studies on the memory differentiation of $CD8^+$ T cells by monocyte-derived dendritic cells during acute infection

2019년 8월

서울대학교 대학원

약학과 의약생명과학전공

신 광 수

Abstract

Studies on the memory differentiation of $CD8^+$ T cells by monocyte-derived dendritic cells during acute infection

Shin, Kwang-Soo

Laboratory of Immunology

Pharmaceutical Bioscience

Department of Pharmacy

The Graduate School

Seoul National University

Monocyte-derived dendritic cells (moDCs) have been shown to robustly expand during infection; however, their roles in anti-infectious immunity remain unclear. Here, I found that moDCs were dramatically increased in the secondary lymphoid organs during acute LCMV infection in an interferon-γ (IFN-γ)-dependent manner. I also found that priming by moDCs enhanced the differentiation of memory $CD8^+$ T cells compared to differentiation primed by

conventional dendritic cells (cDCs) through upregulation of Eomesodermin (Eomes) and T cell factor-1 (TCF-1) expression in $CD8^+$ T cells. Consequently, impaired memory formation of $CD8^+$ T cells in mice that had reduced numbers of moDCs led to defective clearance of pathogens upon rechallenge. Mechanistically, attenuated interleukin-2 (IL-2) signaling in $CD8^+$ T cells primed by moDCs was responsible for the enhanced memory programming of $CD8^+$ T cells. Therefore, these findings unveil a specialization of the antigen-presenting cell subsets in the fate determination of $CD8^+$ T cells during infection and pave the way for the development of a novel therapeutic intervention on infection.

Keywords: Infectious disease, LCMV, Monocyte-derived dendritic cell, IFN-γ, Cellular immunity, Dendritic cell, $CD8^+$ T cell

Student number: 2012-21595

Table of contents

List of Figures

Abbreviations

Ab	Antibody
Ag	Antigen
APC	Antigen-presenting cell
Arm	Armstrong
BHI	Brain heart infusion
Blimp-1	B lymphocyte-induced maturation protein-1
BM	Bone marrow
BMP	Bone marrow progenitor cell
CCR2	C-C chemokine receptor type 2
CD	Cluster of differentiation
cDC	Conventional dendritic cell
CFU	Colony forming unit
CL-13	Clone-13
cMoP	Common monocyte progenitor cell
CTV	Cell trace violet
CX3CR1	C-X3-C motif chenokine receptor 1
ELISA	Enzyme-linked immunosorbent assay

Eomes	Eomesodermin
FACS	Fluorescence-activated cell sorter
GM-CSF	Granumocyte-macrophage colony-stimulating factor
GP	Glycoprotein
GzmB	Granzyme B
i.p.	Intraperitoneally
i.v.	Intravenously
IFN-γ	Interferon gamma
IL	Interleukin
iNOS	Inducible nitric oxide synthase
KLRG1	Killer cell-lectin-like receptor subfamily G member 1
LCMV	Lymphocytic choriomeningitis virus
Lm	Listeria monocytogenes
LN	Lymph node
Ly6	Lymphocyte antigen 6 complex
mAb	monoclonal antibody
MDP	Monocyte-dendritic cell progenitor
MDSC	Myeloid-derived suppressor cell
MHC	Major histocompatibility complex

moDC	Monocyte-derived dendritic cell
MPEC	Memory-precursor effector cell
МΦ	Macrophage
p.i.	Post infection
PBMC	Peripheral blood mononuclear cell
PCR	Polymerase chain reaction
PD-L1	Programmed death-1 ligand 1
PFU	Plaque forming unit
SLEC	Short-lived effector cell
SLO	Secondary lymphoid organ
T-bet	T-box expressed in T cells
TCF1	T cell factor 1
TCR	T cell receptor
TGF	Tumor growth factor
Th	Helper T
TNF	Tumor necrosis factor
Treg	Regulatory T

I. Introduction

I.I. $CD8^+$ T cell responses during infection

$CD8^+$ T cells play prominent roles in defense against infectious pathogens and malignant cancer cells. They respond to infection and inflammation via Ag stimulation from infected cells or antigen-presenting cells (APC) and as a consequent, acquire Ag-specific killing ability. The $CD8^+$ T cell responses can be divided into four-to-five phases **(Figure 1)**(1). At the onset of infection, Ag-specific $CD8^+$ T cells are initially activated by the interaction between naïve $CD8^+$ T cells and APCs (the activation phase). After the activation, $CD8^+$ T cells expand robustly and combat infection (the expansion phase). After the antigen clearance, most of effector $CD8^+$ T cells undergo apoptosis (the contraction phase) and a small number of them which survived during the contraction phase are maintained as memory $CD8^+$ T cell pool (the memory phase). When reinfection occurs, memory $CD8^+$ T cells expand rapidly and clear infectious pathogens faster than during primary infection because they possess an enhanced proliferative capacity and retain their functional properties (the recall response). Thus, inducing sufficient memory $CD8^+$ T cell pool is an important goal of vaccination.

Activated $CD8^+$ T cells can be subdivided into two subsets; short-lived effector cells (SLECs) and memory-precursor effector cells (MPECs) **(Figure 2)**(2). SLECs, which represent the terminally differentiated subset of $CD8^+$ T cells, are characterized by their high expression of KLRG1 and low expression of CD127. They typically comprise more than 90% of effector $CD8^+$ T cell pool at the peak of the expansion phase and are diminished at the contraction phase by apoptotic cell death. MPECs, which can be identified by their high expression of CD127 and low of KLRG1, have multi-potency and undergo further differentiation into memory cells during the contraction phase. The precise mechanisms underlying the diversification of $CD8^+$ T cell fate remain unclear. Howerver, it is evident that the differentiation of $CD8^+$ T cells is directed by the early signals during their activation(3).

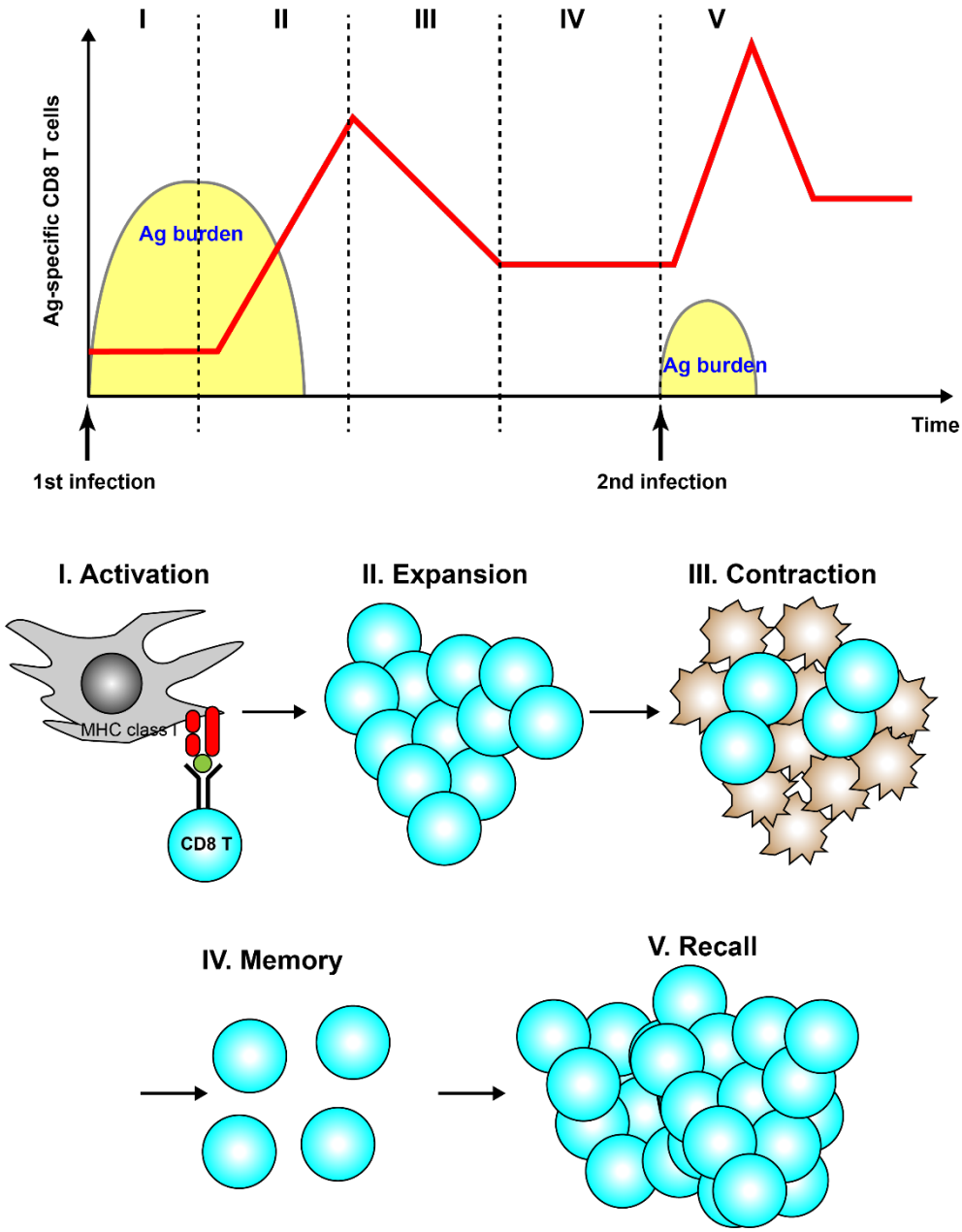

Figure 1. CD8$^+$ T cell responses during infection

CD8$^+$ T cell responses during acute infection can be divided into five distinct phases. CD8$^+$ T cells are activated by APCs and expand robustly thereafter. After the pathogen clearance, CD8$^+$ T cells undergo the contraction phase in which

most of them are diminished and only a small number of them survive. Survived Ag-experienced $CD8^+$ T cells constitute memory T cell pool and protect the host from reinfection.

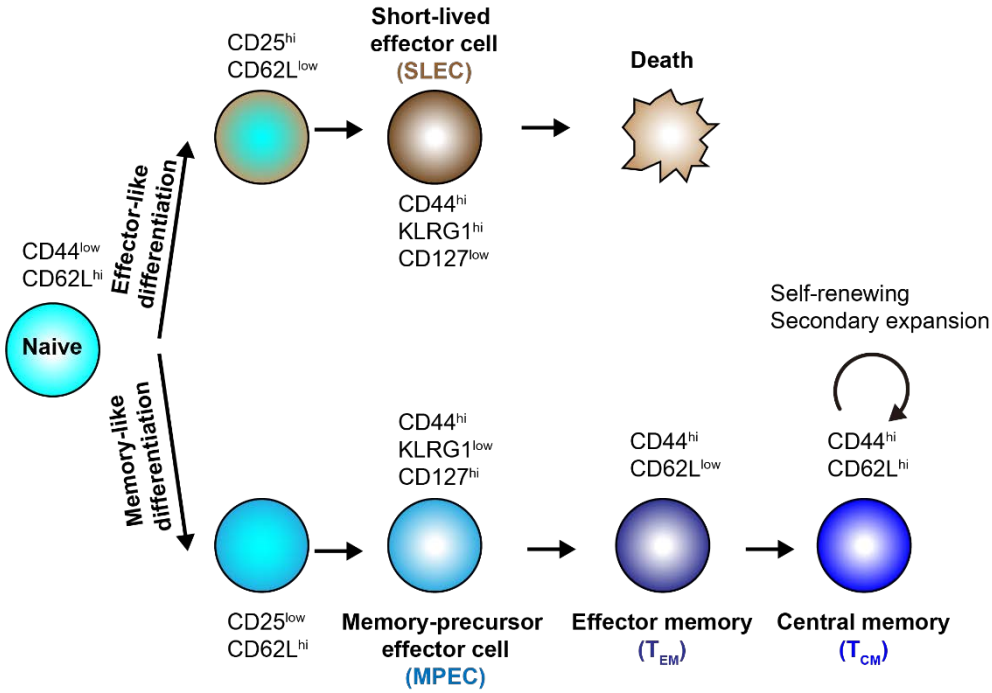

Figure 2. The differentiation of CD8$^+$ T cells during infection

Activated CD8$^+$ T cells experience further differentiation into two subsets. SLECs have superior cytotoxicity and are rapidly diminished in the contraction phase. MPECs survive during the contraction phase and obtain memory cell properties with a self-renewing capacity.

I.II. $CD8^+$ T cell activation

There are three signals responsible for the activation of Ag-specific $CD8^+$ T cells **(Figure 3)**(1, 4, 5). Initially, $CD8^+$ T cells are activated by recognizing the specific Ags on the surface of APCs. T cell receptors (TCRs) on $CD8^+$ T cells bind to the MHC class I molecules on the surface of APCs and CD8 molecules also bind to MHC molecules to stabilize the entire TCR-MHC complex. This event typically takes place in the secondary lymphoid organs (SLOs) (Signal 1). In addition to Signal 1, secondary signals are necessary for $CD8^+$ T cells to become effector cells. This process, so called as costimulation, occurs through APC-bound costimulatory molecules such as CD86, CD80, CD40 (Signal 2). $CD8^+$ T cells also require additional stimulation from different cytokines including IL-2, IL-12, Type I and II interferons (signal 3). Overall, the cooperation of these three signals induces the activation, proliferation and polarization of $CD8^+$ T cells and is critical in the fate-decision of $CD8^+$ T cells.

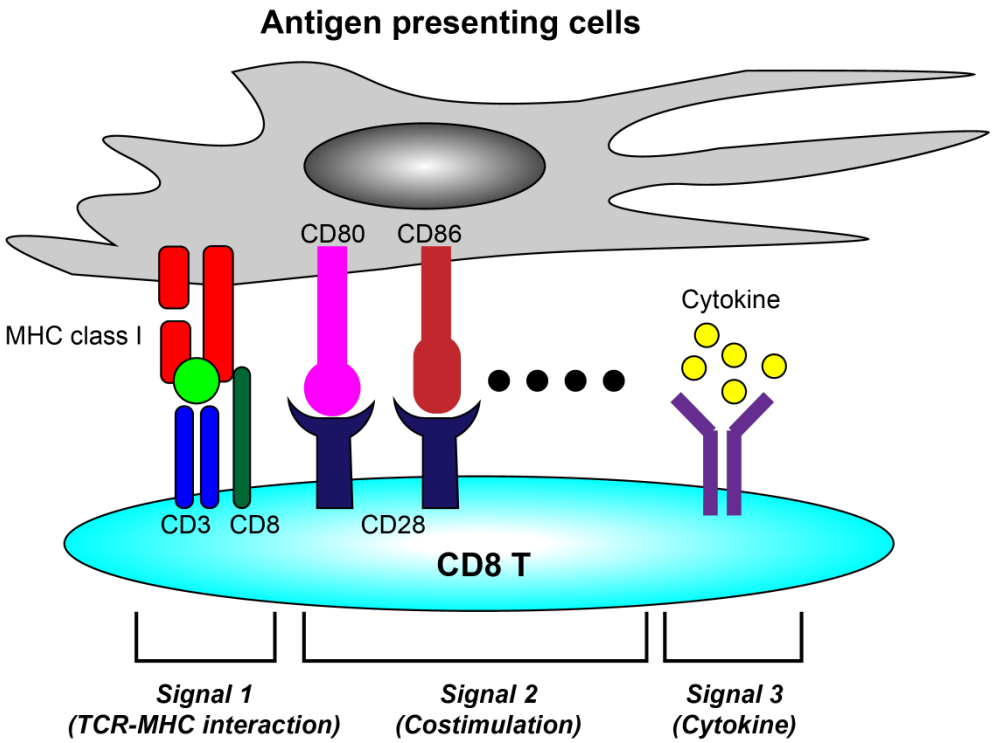

Figure 3. Three signals that involved in CD8$^+$ T cell activation

The activation of CD8$^+$ T cells is governed by the cooperation of three signals; Signal 1 (TCR-MHC interaction), Signal 2 (costimulation) and Signal 3 (cytokine).

I.III. Determinants of CD8$^+$ T cell fate

It is evident that the CD8$^+$ T cell differentiation is dictated by different non-mutually exclusive factors(3). TCR signal quantity and quality induce the diversification of progeny from a single CD8$^+$ T cell(6). A strong TCR signal diverts CD8$^+$ T cells to undergo effector-prone differentiation, whereas a weak TCR signal licenses CD8$^+$ T cells to differentiate into memory-like cells. Recent studies have proposed that complex transcriptional regulations are involved in these events. For example, T-bet and Blimp-1 have been shown to promote terminal differentiation of effector CD8$^+$ T cells, while Eomes and TCF1 are associated with memory-like differentiation **(Figure 4)**(2, 7-9). Additionally, differences in the cytokine milieu around an individual CD8$^+$ T cell can contribute to its fate determination(10). IL-12, IL-15 and type I IFNs have been shown to induce the robust activation and proliferation of effector CD8$^+$ T cells on the early phase of infection(2, 11). IL-2 is also required for the optimal amplification of CD8$^+$ T cell population and SLEC differentiation(12). During the contraction phase of CD8$^+$ T cell response, TGF-β has been suggested to play a critical role in inducing apoptotic cells death of SLECs **(Figure 5)**(13).

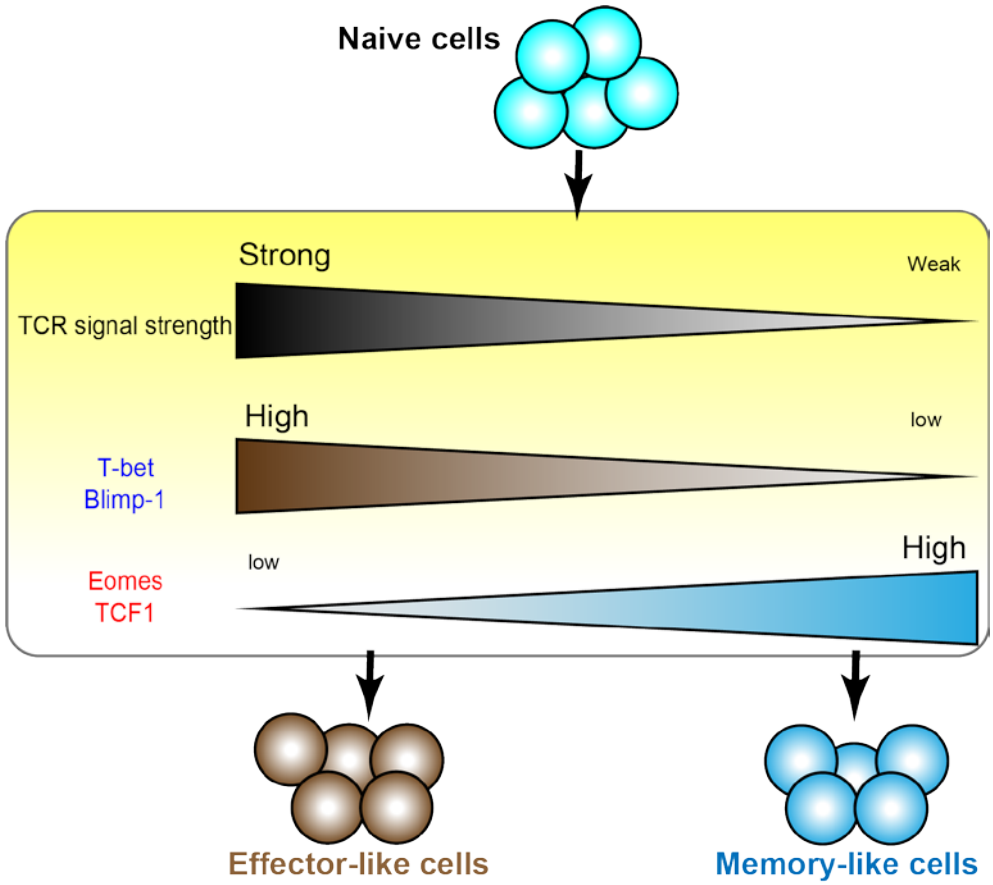

Figure 4. Determinants of CD8$^+$ T cell fate

The TCR signal strength is a critical determinant of CD8$^+$ T cell fate upon activation. A strong TCR signal induces CD8$^+$ T cells to elevate T-bet/Blimp-1 expression and to differentiate into effector-like cells. In contrast, a weak TCR signal drives CD8$^+$ T cells to express high levels of Eomes/TCF1 and directs them to memory-like cells subsequently.

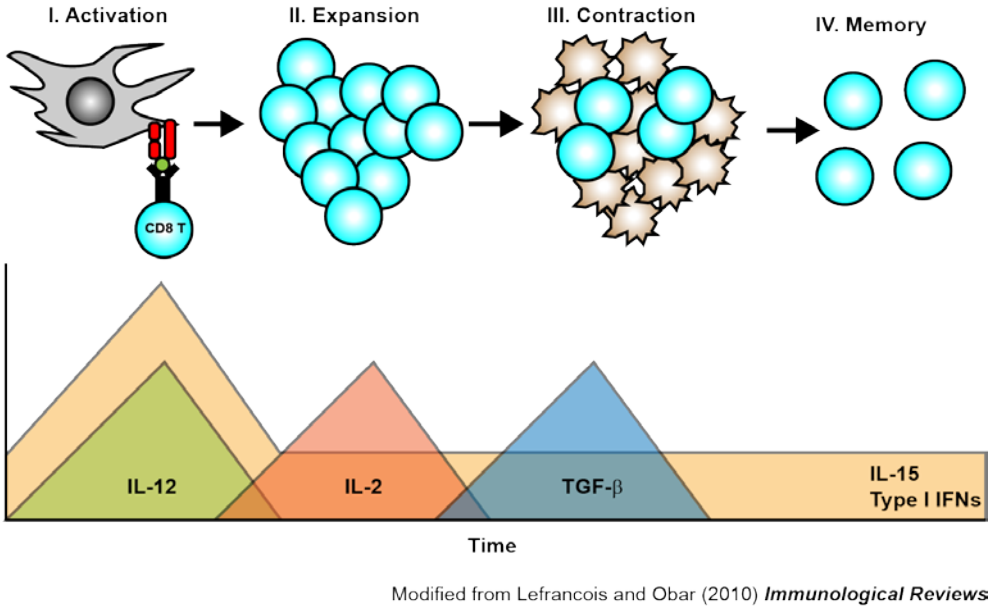

Figure 5. Cytokine signals in CD8$^+$ T cell differentiation

Different cytokines have been known to be associated with CD8$^+$ T cell differentiation. IL-12, IL-15 and type I IFNs are crucial for the expansion of CD8$^+$ T cells and the differentiation of SLECs. IL-2 also takes part in the optimal expansion of effector CD8$^+$ T cells. TGF- β has been shown to be involved in the apoptosis of SLECs(10).

I.IV. Emergency myelopoiesis

Emergency myelopoiesis frequently occurs during infection and inflammation(14, 15), in which innate myeloid cells robustly expand and are recruited to the inflamed sites to clear pathogens or infected cells **(Figure 6)**. Among them, the mononuclear phagocyte system (MPS) composed of conventional dendritic cells (cDCs), macrophages (MΦs) and monocytes is known to play a crucial role not only in innate immune responses but also in adaptive immune responses via Ag presentation to T cells **(Figure 7)**(16). However, their respective definition and role in infections are still confused because they commonly share surface markers, ontogeny and functions(17). For example, MΦs, which take part in the clearance of cellular debris and pathogens, have been thought to be derived from hematopoietic progenitors. However, it has recently become evident that adult tissue macrophages mainly develop from yolk sac (or fetal liver)-derived progenitor cells during embryogenesis(18). Thus, the differentiation and function of monocytes during infection remain to be further investigated(19).

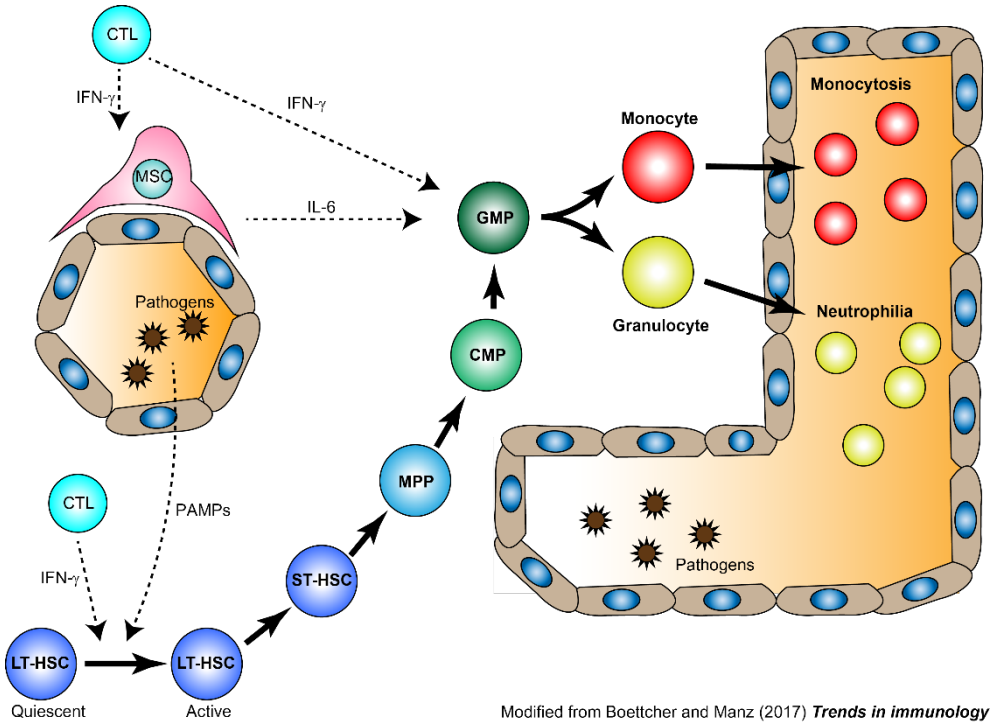

Figure 6. Integrated model of emergency myelopoiesis during infection

IFN-γ secreted from $CD8^+$ T cells promotes emergency myelopoiesis by acting on granulocyte-macrophage progenitor cells (GMPs) as well as by stimulating mesenchymal stromal cells (MSCs) to secrete IL-6(20). IFN-γ can stimulate hematopoietic stem cells (HSCs), thereby triggering them to enter the cell cycle. Pathogen-associated molecular patterns (PAMPs) induce the proliferation of HSCs as well. Consequently, stimulated HSCs and their progeny progenitor cells are differentiated into myeloid cells(14).

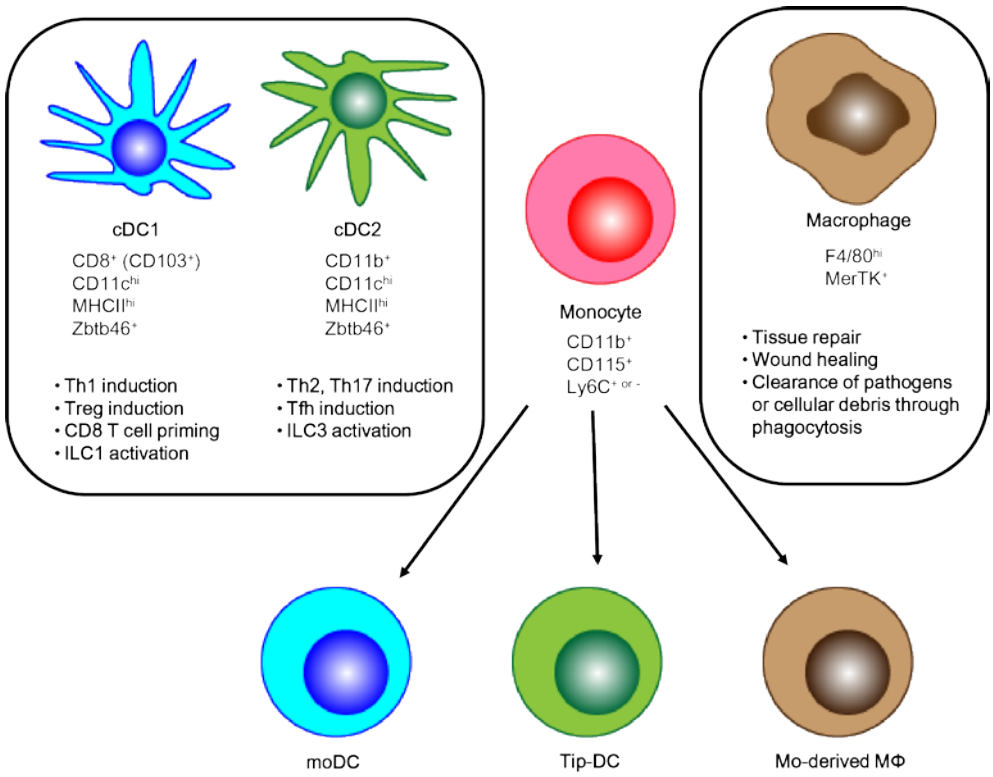

Figure 7. Mononuclear phagocyte system

MPS is composed of cDCs, MΦs and monocytes. cDCs can be divided into two subpopulations; $CD8^+$ ($CD103^+$) cDC1 and $CD11b^+$ cDC2, which have the potential to induce Th1 and Th2 responses, respectively. MΦs play a crucial role in the defense against infection through their enhanced phagocytic ability. Monocytes also contribute to the link between innate and adaptive immune responses. Moreover, monocytes can further differentiate into DC- or MΦ-like cells.

I.V. Monocytes and monocyte-derived dendritic cells

Murine monocytes can be classified into two subsets; Ly6C$^+$ circulating monocytes and Ly6C$^-$ patrolling monocytes. After egressing from the BM, Ly6C$^+$ monocytes emigrate to inflamed tissue and draining lymph nodes while Ly6C$^-$ monocytes remain in the vasculature(21). During infection and inflammation, Ly6C$^+$ monocytes further differentiate into DC-like cells, which are coined as monocyte-derived DCs (moDCs) or TNF and iNOS producing DCs (Tip-DCs) depending on the context(22, 23). Previous reports have proposed that common monocyte progenitor cells (cMoPs) in the bone marrow (BM) are a progenitor of moDCs(24, 25). However, the specific mechanism that drives the differentiation of moDCs from cMoPs remains to be elucidated.

As monocytes and moDCs preferentially populate the antigen-presenting cell (APC) pool during infection and inflammation, their roles in inducing T cell responses have been studied in several models; they trigger Th1 responses in response to infections and allogeneic stimulation(26-29), Th2 responses in house dust mite-induced asthma(30), Th17 responses in autoimmune diseases(31) and Treg generation in cancer(32). Monocytes and moDCs are also known to affect CD8$^+$ T cell responses despite conflicting results from various animal models. For example, tumor-infiltrating moDCs have been shown to prime CD8$^+$ T cells

and induce anti-tumor immunity(25). In contrast, monocytic cells in chronic infections abrogate the induction of anti-infectious $CD8^+$ T cell responses **(Figure 8)**(33). Therefore, how monocytes and moDCs contribute to the differentiation of $CD8^+$ T cells remains elusive.

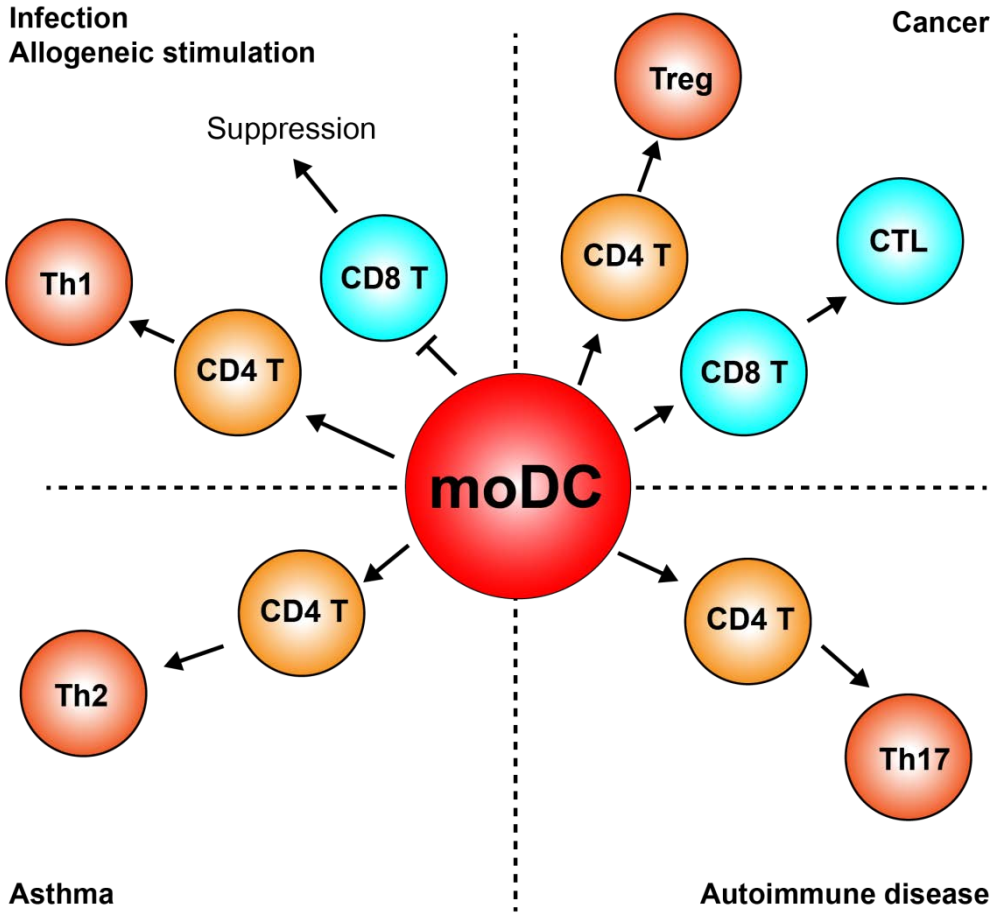

Figure 8. The roles of moDCs in different experimental models

moDCs trigger Th1 responses in response to infections and allogeneic stimulation, Th2 responses in house dust mite-induced asthma, Th17 responses in autoimmune diseases and Treg generation in cancer. They are also known to affect $CD8^+$ T cell responses. Tumor-infiltrating moDCs have been shown to prime $CD8^+$ T cells and induce anti-tumor immunity. In contrast, monocytic cells

in chronic infections abrogate the induction of anti-infectious $CD8^+$ T cell responses.

I.VI. The purpose of this study

Although the TCR signal strength is strongly influenced by the signals delivered by APCs to $CD8^+$ T cells and there are various types of APCs in SLOs during infection, the contributions of each APCs on the diversification of $CD8^+$ T cell fate remain relatively unknown. Despite a recent study which has clearly demonstrated the contribution of $CD103^+$ cDCs (cDC1) to effector $CD8^+$ T cell differentiation(34), the specific APC types that license memory $CD8^+$ T cell differentiation still necessitate further investigation.

In this report, I investigated the role of moDCs in memory $CD8^+$ T cell differentiation during acute infection. I found that moDCs were expanded during *Lymphocytic Choriomeningitis virus* (LCMV) infection, and common monocyte progenitor cells (cMoPs) among BM progenitor cells (BMPs) differentiated into moDCs in an IFN-γ-dependent manner. Of interest, $CD8^+$ T cells primed in the absence of moDCs could not develop into memory cells properly, while they underwent effector-prone differentiation during the expansion phase of infection. These results suggest a crucial role of moDCs in the generation of memory T cell pool, which has implications for the development of novel vaccine strategies against infection.

II. Materials and Methods

Animals

C57BL/6J mice were purchased from the Institute of Medical Science at the University of Tokyo and Balb/c mice from Charles River Laboratory. OT-I (C57BL/6-Tg(TcraTcrb)1100Mjb/J), P14 (B6;D2-Tg(TcrLCMV)327Sdz/JDvsJ), *Ccr2*$^{-/-}$ (B6.129S4-Ccr2^{tm1Ifc}/J), *Ifng*$^{-/-}$ (C.129S7(B6)-Ifng^{tm1Ts}/J) and CD45.1 (B6.SJL-Ptprc^{a}Pepc^{b}/BoyJ) mice were purchased from Jackson Laboratory. CD45.1^{+} P14 mice were obtained by crossbreeding CD45.1^{+} mice and C57BL/6J mice. Age (6 to 12 weeks) and sex-matched mice were used for all experiments. All mice were bred and maintained under specific pathogen-free conditions in the Animal Facility of Seoul National University. Experiments with infectious pathogen were performed in the ABL2 vivarium of Seoul National University. All animal protocols were reviewed and approved by the Institutional Animal Care and Use Committee (IACUC) of Seoul National University.

Infections, IFN-γ neutralization and tissue titrations

For primary infection, mice were injected intraperitoneally (i.p.) with LCMV-Arm (2×10^5 plaque-forming units (PFU)) or intravenously (i.v.) with GP_{33-41}-

expressing *Listeria monocytogenes* (Lm-GP33, 5000 colony-forming units (CFU)), which were generously donated from Yonsei University. To analyze the host protection capacity of memory cells, mice were infected with Lm-GP33 (5000 CFU). To neutralize IFN-γ *in vivo*, mice were treated i.p. with 500 μg anti-IFN-γ mAb (HB170, ATCC) at day 1, 4 and 7 p.i. for LCMV-Arm infection, and at day -1 and 1 p.i. for Lm-GP33 infection.

Tissue titrations were conducted as previously described(35). In brief, spleens were obtained from Lm-GP33-infected mice, prepared as a single-cell suspension, and then treated with 1% Triton X-100 solution (Sigma-Aldrich). Each diluted suspension was plated on BHI agar plates (BD Biosciences) and incubated overnight at 37 °C. Colonies on the plates were counted the next day, and titers were calculated as CFUs per gram of spleen.

Flow cytometry

Spleen and peripheral lymph nodes were isolated from mice and homogenized using a 70 μm cell strainer (BD Biosciences). Bone marrow cells were isolated by flushing the tibia and femur of mice with a 1-ml syringe. PBMCs in the blood were isolated using Hispaque-1077 (Sigma-Aldrich, St. Louis, MO, USA) following the manufacturer's protocol. Red blood cells (RBC) of single cell

suspensions were lysed using RBC Lysis Buffer (eBioscience).

Abs used for flow cytometry were as follows: anti-IA/IE (M5/114.15.2), anti-CD11b (M1/70), anti-CD11c (N418), anti-Ly6G (1A8), anti-Ly6C (HK1.4), anti-CCR2 (475301, R&D Systems), anti-CX3CR1 (SA011F11), anti-F4/80 (BM8, eBioscience), anti-CD64 (X54-5/7.1), anti-CD115 (AFS98), anti-CD135 (A2F10), anti-CD119 (2E2), anti-CD45.1 (A20), anti-CD45.2 (104), anti-H-$2K^b$ (AF6-88.5), anti-H-D^b (KH95), anti-CD40 (3/23), anti-CD80 (16-10A1), anti-CD86 (GL-1), anti-PD-L1 (10F.9G2), anti-CD8α (53-6.7), anti-CD3ε (145-2C11), anti-CD25 (PC61), anti-CD62L (MEL-14), anti-KLRG1 (2F1/KLRG1), anti-CD127 (A7R34), anti-IFN-γ (XMG1.2), anti-TNF-α (MP6-XT22), anti-granzyme B (GB11), anti-Eomes (Dan11mag, eBioscience), anti-T-bet (4B10, eBioscience) and anti-TCF1 (C63D9, Cell Signaling). Abs were purchased from BioLegend unless otherwise described. Streptavidin-APC/Cy7 (BioLegend) and Alexa Fluor 647 goat anti-rabbit IgG (Invitrogen) were used for secondary staining.

Single cell suspensions were stained for surface molecules for 30 minutes at 4 °C. Dead cells were excluded from analysis using Fixable Viability Dye (eBioscience). For intracellular cytokine staining, cells were restimulated with GP_{33-41} peptide (KAVYNFATC, 0.2 μg/ml, Genscript) in the presence of BD

GolgiPlug (BD Biosciences) for 4 hours, fixed and permeabilized using a Cytofix/Cytoperm kit (BD Biosciences) according to the manufacturer's instructions. To detect transcription factors, a fixation/permeabilization kit purchased from eBioscience was used. For analyzing cellular apoptosis, FITC Annexin V apoptosis Detection Kit I and Propidium Iodide Staining Solution (BD Biosciences) were used. Samples were collected using a FACS LSRFortessa X-20 or FACS Aria III (BD Biosciences), and data were analyzed with FlowJo software (Treestar).

Cell sorting

For sorting BMPs, BM cells of naïve mice were labeled with biotinylated anti-CD3ε, anti-CD19, anti-CD49b and anti-Ly6G (all from Biolegend) followed by anti-biotin microbeads (Miltenyi Biotech) and isolated using a MACS LD column (Miltenyi Biotech). The collected cells were further sorted into each BMP subset: total BMPs ($lin^-c\text{-}kit^+CD11b^-Ly6C^-$), cMoPs ($lin^-c\text{-}kit^+CD115^+CD135^-CD11b^-Ly6C^+$), MDPs ($lin^-c\text{-}kit^+CD115^+CD135^+CD11b^-Ly6C^-$), $CD135^+$ BMPs ($lin^-c\text{-}kit^+CD115^-CD135^+CD11b^-Ly6C^-$) and $CD115^-CD135^-$ BMPs ($lin^-c\text{-}kit^+CD115^-CD135^-CD11b^-Ly6C^-$).

To isolate cDCs and moDCs from infected mice, Lin^- cells of infected

splenocytes (day 4 or day 8 p.i.) were isolated using a MACS LD column and further sorted to each subset (cDCs as lin$^-$IA/IE$^+$CD11c$^+$CD11b$^-$CCR2$^-$Ly6C$^-$ and moDCs as lin$^-$IA/IE$^+$CD11c$^{-/int}$CD11b$^+$CCR2$^+$Ly6C$^+$).

CD45.1$^+$ P14 cells used in the *in vitro* and *in vivo* experiments were enriched using anti-CD8a microbeads and a MACS LS column (Miltenyi Biotech) and further purified to CD45.1$^+$CD8$^+$ cells by cell sorting.

Cell sorting was conducted using a FACS Aria II or FACS Aria III. The purities of all sorted populations were greater than 95%.

ELISA

The IFN-γ concentration in mouse serum was measured using a mouse IFN-γ ELISA kit (BD Biosciences) according to the manufacturer's protocol. The IL-2 concentrations in the cocultures of T cells and APCs were measured using the following Abs: anti-IL-2 (JES6-1A12) for capture, biotinylated anti-IL-2 (JES6-5H4) and streptavidin-HRP for detection (all from BD Biosciences).

BM cell differentiation assay

To evaluate the differentiation patterns of BMPs *in vitro*, sorted total BMPs, cMoPs, MDPs, CD135$^+$ BMPs and CD115$^-$CD135$^-$ BMPs (1×10^4 cells/well)

were cultured for 4 to 6 days under specific conditions as follows: GM-CSF, GM-CSF plus IL-4 or GM-CSF plus IFN-γ (all from R&D systems). All recombinant cytokines were used at 20 ng/ml, and the culture medium was refreshed every 2 days.

To analyze the differentiation patterns of cMoPs *in vivo*, sorted cMoPs and non-cMoPs (2×10^5 cells each/mouse) were adoptively transferred to LCMV-Arm infected recipient mice at day 5 p.i. Donor cells were analyzed at day 3 post transfer (day 8 p.i.).

In vitro APC:T cell coculture and in vitro cytotoxicity assay

The 1×10^4 APCs (cDCs or moDCs) and 5×10^4 P14 cells were cultured for 3 days in the presence of GP_{33-41} peptide. To determine the proliferation capacity of P14 cells, the cells were labeled with 5 μM of CellTrace Violet (CTV, Invitrogen) for 15 minutes prior to incubation. The cocultures in some experiments were treated with recombinant mouse IL-2 (10 ng/ml, Peprotech) or anti-IL-2 mAbs (10 μg/ml, JES6-1A12, eBioscience).

To measure the cytotoxicity of activated $CD8^+$ T cells, equivalent numbers of purified live effector P14 cells from *in vitro* cocultures or infected mice were cocultured with ^{51}Cr-labeled GP_{33-41}-loaded EL4 cells (ATCC) for 4 hours. Target

cell specific lysis was measured by a Wallac 1470 Wizard automatic γ-counter (PerkinElmer) and calculated using the following equation; [(sample lysis count per minute (CPM) – spontaneous lysis CPM) / (Triton X-100-mediated lysis CPM – spontaneous lysis CPM)] × 100 (%).

T cell adoptive transfer

To examine the primary immune responses, 1×10^4 purified $CD8^+$ P14 cells from P14 splenocytes were adoptively transferred into WT or *Ccr2*$^{-/-}$ mice and analyzed at the indicated time points. To establish the memory of P14 cells, 1×10^6 P14 cells isolated from infected mice at day 8 p.i. were adoptively transferred to naïve recipient mice. To evaluate the memory-generation capacity of P14 cells primed by moDCs and cDCs *in vitro*, P14 cells were activated as indicated in the 'In vitro APC:T cell coculture' section and then transferred to infected mice at day 8 p.i. (5×10^5 cells/mouse).

Quantitative real-time PCR

Total RNA of sorted P14 cells from infected mice at day 8 p.i. was isolated using TRIzol reagent and reverse-transcribed into cDNA using AmfiRivert II cDNA

Synthesis Master Mix (Gendepot). Real-time PCR was performed with a SYBR Green real-time PCR kit (Takara) and LightCycler 1.5 instrument (Roche Diagnostics). Primers were purchased from Cosmo Genetech, and their sequences were as follows: mouse *Tbx21* (forward; 5'– ACA AGG GGG CTT CCA ACA AT –3', reverse; 5'– TGC GTT CTG GTA GGC AGT CA –3'), mouse *Eomes* (forward; 5'– AGA ACC GTG CCA CAG ACC AA –3', reverse; 5'– TCG TCA CAG GTT GCT GGA CA –3'), mouse *Tcf7* (forward; 5'– GCA CAC TTC GCA GAG ACT TT –3', reverse; 5'– GTG GAC TGC TGA AAT GTT CG –3'), mouse *Prdm1* (forward; 5'– ACT CAG TCG CAT TTG ATG GC –3', reverse; 5'– GGT CAG TAA GGC TCT TGG GT –3'), mouse *Il2* (forward; 5'– CAA CTG TGG TGG ACT TTC TG –3', reverse; 5'– CCT TGG GGC TTA CAA AAA GAA –3') and mouse *Hprt* (forward; 5'– AAG ACT TGC TCG AGA TGT CAT GAA –3', reverse; 5'– ATC CAG CAG GTC AGC AAA GAA –3'). The value of each gene expression level was normalized to the expression level of mouse *Hprt*.

Statistics

Statistical analysis of all data was conducted using GraphPad Prism 5 software (GraphPad Software, Inc.). The unpaired, two-tailed Student's t test was used to compare two groups and one-way ANOVA with Bonferroni's multiple

comparisons was used to compare more than three groups. Two-way ANOVA with Bonferroni's multiple comparisons was used in Figures 10E and 12. P values<0.05 were considered significant.

III. Results

III.I. IFN-γ-dependent expansion of monocyte-derived dendritic cells during acute viral infection

Various types of APCs in inflamed tissues and lymphoid organs are known to initiate adaptive immune responses during infection. Among those APCs, I sought to determine the role of moDCs in anti-infectious immune responses. First, I investigated the frequencies and numbers of moDCs and cDCs in lymphoid organs after acute LCMV (LCMV-Arm) infection. Based on a previous report(29), cDCs and moDCs in the spleen were defined by their cell surface marker expression patterns; $Ly6G^{-}IA/IE^{+}CD11c^{hi}CD11b^{low/hi}Ly6C^{-}CCR2^{-}$ cells and $Ly6G^{-}IA/IE^{+}CD11c^{low/int}CD11b^{hi}Ly6C^{+}CCR2^{+}$ cells, respectively. moDCs were sparsely present in uninfected mice, while cDCs represented a dominant APC subset at steady state. However, moDCs rapidly accumulated in the spleen after LCMV-Arm infection and became an abundant APC population during the expansion phase of infection **(Figures 9A and 9B)**. In addition, high expression levels of F4/80, CD64 and CX3CR1 in moDCs compared to those in cDCs indicated that moDCs were distinct from cDCs **(Figure 9C).**

I further investigated the underlying mechanism of the accumulation of moDCs during infection. Recent reports have demonstrated that IFN-γ induces the differentiation, migration and expansion of inflammatory monocyte lineage cells during infection (36-38). In this regard, the level of serum IFN-γ was elevated in LCMV-Arm-infected mice approximately 2 days prior to the accumulation of moDCs **(Figure 10A)**. To determine whether the accumulation of moDCs was regulated by IFN-γ, I treated infected mice with IFN-γ–neutralizing Ab **(Figure 10B)**. IFN-γ neutralization led the slight increase in the viral loads in mice **(Figure 10C)**(39). Although the absolute numbers of cDCs and moDCs were decreased along with reductions in the numbers of splenocytes, I found that the frequency of moDCs was markedly reduced in the spleen of mice that received IFN-γ–neutralizing Ab, while the frequency of cDCs did not decrease significantly **(Figures 10D and 10E)**. Importantly, moDCs were almost completely absent in the BM of LCMV-Arm-infected mice with neutralized IFN-γ **(Figure 10F)**. IFN-γ neutralization did not lead to the reductions of BMPs, but it rather induced the enhanced BMP frequencies **(Figure 11A)**. Furthermore, IFN-γ neutralization did not induce apoptotic death of moDCs **(Figure 11B)**. Thus, I concluded that the IFN-γ-dependent accumulation of moDCs in the periphery is due to the increased generation of the cells rather than the enhanced

migration from the BM, their enhanced survival, or the effects of IFN-γ on the frequencies of BMPs. I also confirmed that IFN-γ is required for moDC generation in the spleen and BM during LCMV-Arm infection using IFN-γ-deficient mice **(Figure 12A)**. Additionally, I found that the frequency of moDCs was also increased in GP_{33-41}-expressing *Listeria monocytogenes* (Lm-GP33)-infected mice **(Figures 12B and 12C)**. Consistent with the result on LCMV-Arm infection, accumulation of moDCs was dependent on IFN-γ during Lm-GP33 infection **(Figures 12B and 12C)**. Altogether, these results indicate that moDCs robustly expand in an IFN-γ-dependent manner during an acute viral and bacterial infection.

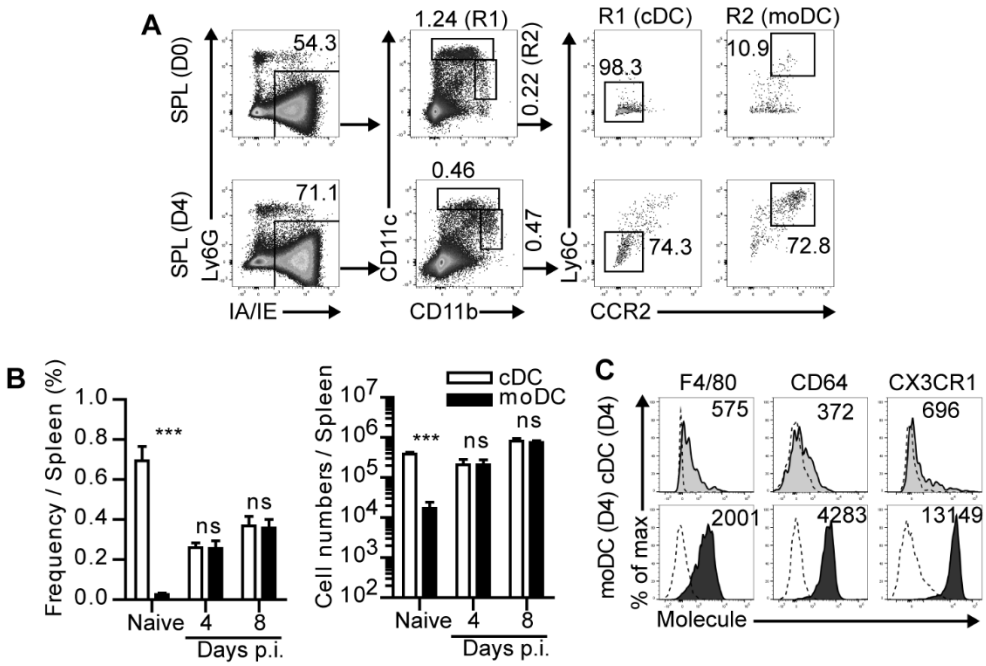

Figure 9. moDCs expand robustly during LCMV-Arm infection

(**A**) Gating strategies of cDCs and moDCs in the spleen of naïve or LCMV-Arm-infected mice. Numbers indicate the percentages of the gates. (**B**) Cell numbers and frequencies of cDCs and moDCs in the spleen during LCMV-Arm infection. (**C**) Expression patterns of surface molecules on cDCs and moDCs in LCMV-Arm infected mice at day 4 p.i. Numbers indicate the MFI values of each molecule. Data are representative of three independent experiments and are shown as the mean±SEM. n=5 per group at each time point. ***$p<0.001$.

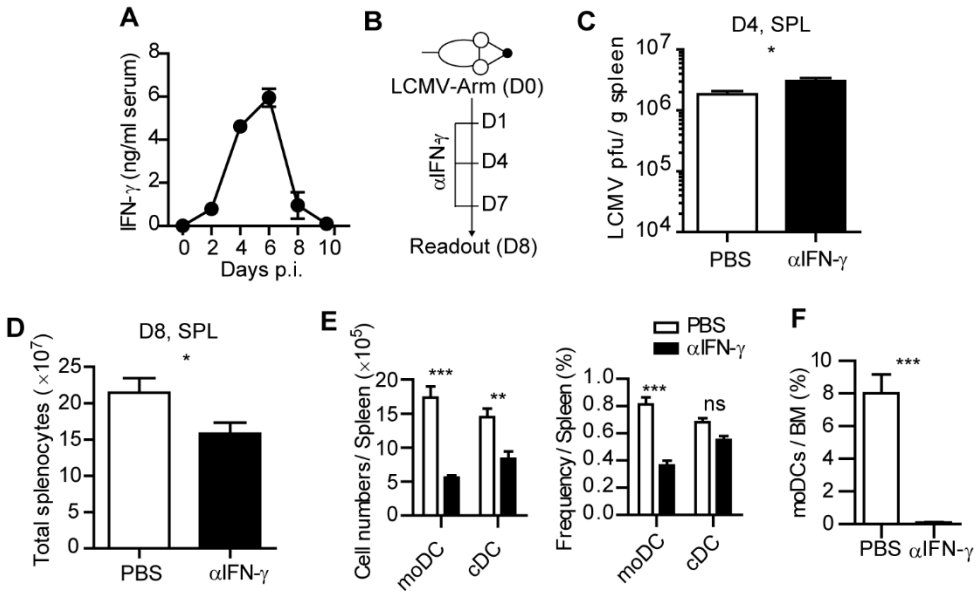

Figure 10. IFN-γ neutralization leads the diminished accumulation of moDCs

(**A**) Kinetics of IFN-γ levels in the serum of LCMV-Arm-infected mice. (**B-F**) LCMV-Arm-infected mice were treated with IFN-γ–neutralizing Ab. (**B**) Experimental schedule. (**C**) Viral titers in the spleen of the mice that received IFN-γ–neutralizing Abs or not were calculated by the plaque assay at day 4 p.i. **(D)** Splenocyte numbers of the mice received IFN-γ–neutralizing Abs or not. (**E**) Cell numbers (left) and frequencies (right) of cDCs and moDCs were measured in the indicated organs on day 8 p.i. and are shown as graph plots. (**F**) Frequency of moDCs in the BM. Data are representative of three independent experiments and are shown as the mean±SEM. n=5 per group at each time point. *p<0.05; **p<0.01; ***p<0.001.

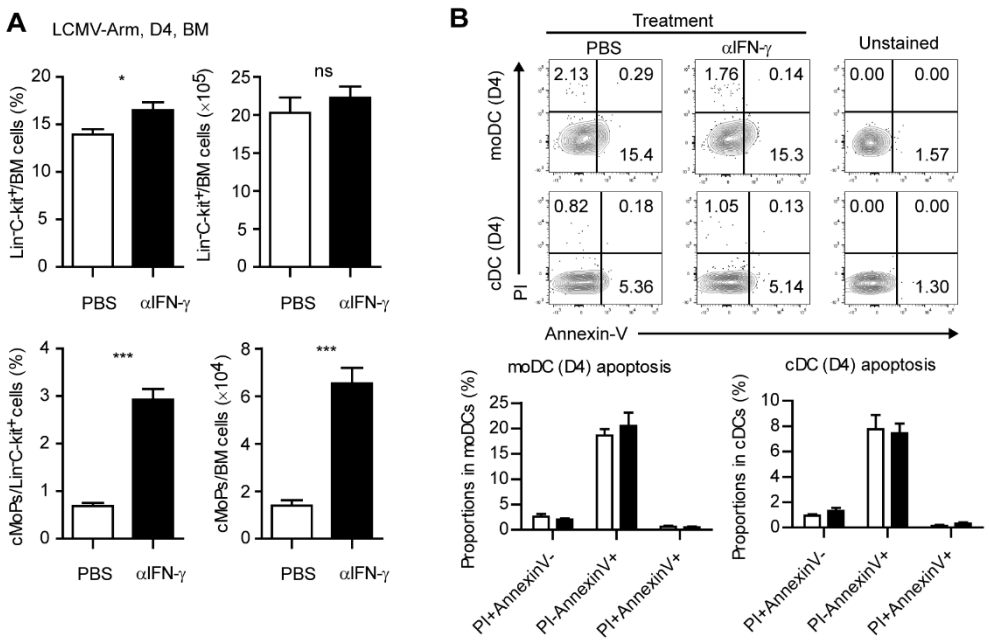

Figure 11. IFN-γ neutralization-induced changes in LCMV-Arm-infected mice

Mice were treated IFN-γ–neutralizing Ab followed by LCMV-Arm infection as depicted in Figure 10B. (**A**) Cell numbers and frequencies of $Lin^{-}C\text{-}kit^{+}$ BM progenitor cells and cMoPs in the BM of mice. (**B**) Propidium Iodide (PI) and Annexin-V stainings of moDCs and cDCs from infected mice that received IFN-γ–neutralizing Abs or not. Representative flow cytometry plots (upper) and graph plots (lower). Numbers in the flow cytometry plots indicate the percentages within the gates. n=5 or 6 per group. Data are shown as the mean±SEM. *p<0.05; **p<0.01; ***p<0.001.

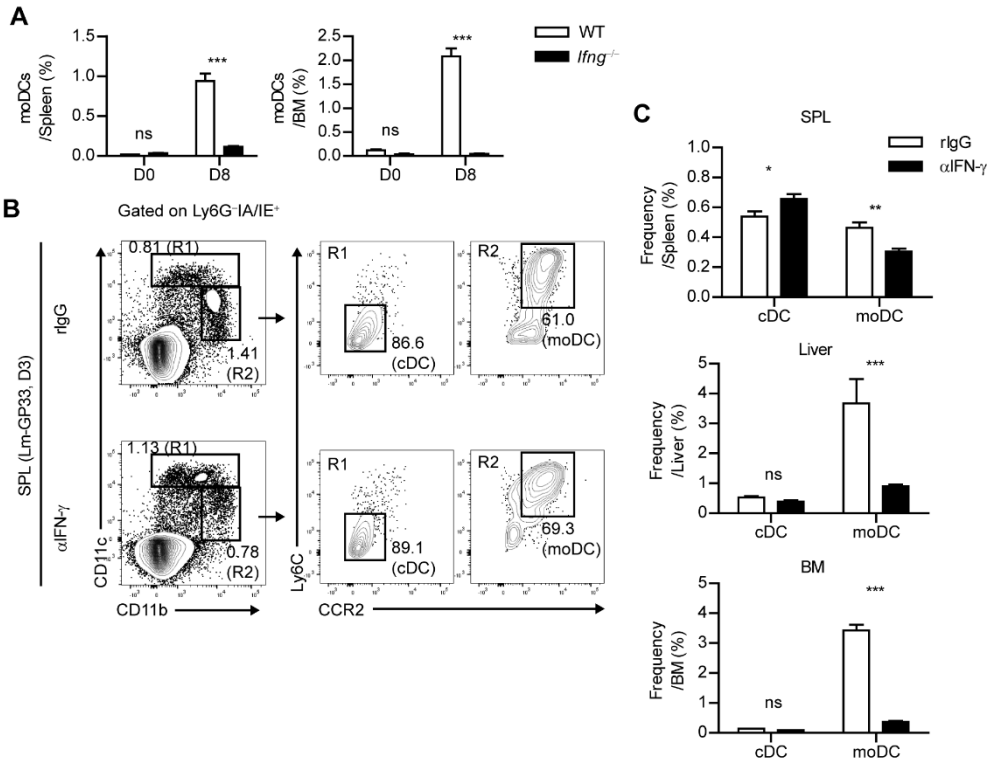

Figure 12. IFN-γ-dependent expansion of moDCs during infection

(**A**) WT and *Ifng*$^{-/-}$ mice were infected with LCMV-Arm, and analyzed on day 8 p.i. Graphs of the frequencies moDCs in the spleen and BM are shown. n=3 per group. (**B and C**) Mice were infected by Lm-GP33 followed by the neutralization of IFN-γ with mAbs. The frequencies of cDCs and moDCs on day 3 p.i. are shown as flow cytometry plots (**B**) and graphs (**C**). Numbers in the flow cytometry plots indicate the percentage within each gate. n=5 per group. Data are representative of two independent experiments and are shown as the mean±SEM. *p<0.05;**p<0.01; ***p<0.001.

III.II. IFN-γ acts directly on common monocyte progenitor cells and promotes the differentiation of moDCs

The observed role of IFN-γ in the surge of moDCs in the periphery after acute infection prompted me to investigate whether IFN-γ could affect moDC generation from specific bone marrow progenitor cells (BMPs). To achieve this goal, I sorted $lin^{-}c\text{-}kit^{+}$ BMPs, differentiated them with GM-CSF, GM-CSF plus IL-4, or GM-CSF plus IFN-γ, and analyzed the differentiation patterns of BMPs at day 5 after culture **(Figure 13A)**. In line with a previous report, BMPs cultured with GM-CSF were differentiated into two distinct populations; GM-Macs ($CD11c^{+}IA/IE^{int}$) and GM-DCs ($CD11c^{+}IA/IE^{hi}$), which represent monocyte-derived macrophages and dendritic cells, respectively(40). While the addition of IL-4 favors differentiation into GM-DCs, IFN-γ promoted the differentiation of BMPs into $Ly6C^{+}CD11b^{+}$ cells instead of GM-Macs or GM-DCs **(Figure 13B)**. Collectively, these results demonstrate that IFN-γ diverts the fate of BMPs from GM-Macs or GM-DCs to moDCs.

Next, I examined the target cells among BMPs that responded directly to IFN-γ. BMPs can be subdivided into four subpopulations by their cell surface expression of CD115 (M-CSFR) and CD135 (Flt3): $CD115^{-}CD135^{+}$ cells as $CD135^{+}$ BMPs, $CD115^{+}CD135^{+}$ cells as monocyte-DC progenitors (MDPs),

$CD115^+CD135^-$ cells as common monocyte progenitors (cMoPs) and $CD115^-$ $CD135^-$ cells as resting $CD115^-CD135^-$ BMPs, which expressed different levels of Ly6C and CD11b **(Figure 14A)**. Interestingly, only cMoPs displayed a high expression level of IFN-γR (CD119) compared with the other populations **(Figure 14B)**. I isolated these cells and differentiated each subpopulation in the presence of GM-CSF and IFN-γ **(Figure 15A)**. In line with the CD119 expression, only cMoPs differentiated immediately into $CD11b^+IA/IE^+Ly6C^+Ly6G^-$ moDC phenotype cells in response to IFN-γ and maintained their phenotype during culture **(Figures 15B and 15C)**. Of note, other populations differentiated into moDCs, to a lesser extent, beginning at day 3 after culture, implying the developmental hierarchy of BMPs. Thus, these results strongly suggest that moDCs are primarily induced from cMoPs in the BM in response to increased IFN-γ after acute viral infection.

To directly investigate whether cMoPs could differentiate into moDCs, I sorted cMoPs and other resting BMPs (non-cMoPs) from the BM of naive mice. Then, I adoptively transferred each BMP cell type into LCMV-Arm infected congenically marked ($CD45.1^+$) recipient mice on day 5 post infection, when IFN-γ was abundant during infection. The frequencies of moDCs among donor cells were analyzed 3 days later **(Figure 16)**. Consistent with the *in vitro*

experiments, the majority of cMoPs differentiated into moDCs, while non-cMoPs showed limited differentiation into moDCs. Taken together, these data suggest that IFN-γ acts directly on cMoPs to promote their differentiation into moDCs in LCMV Arm-infected mice. The accumulation of cMoPs in mice that received IFN-γ–neutralizing Ab **(Figure 11A)** could be explained by these results; cMoPs rarely received IFN-γ signaling, could not develop into moDCs, and consequently accumulated in the BM.

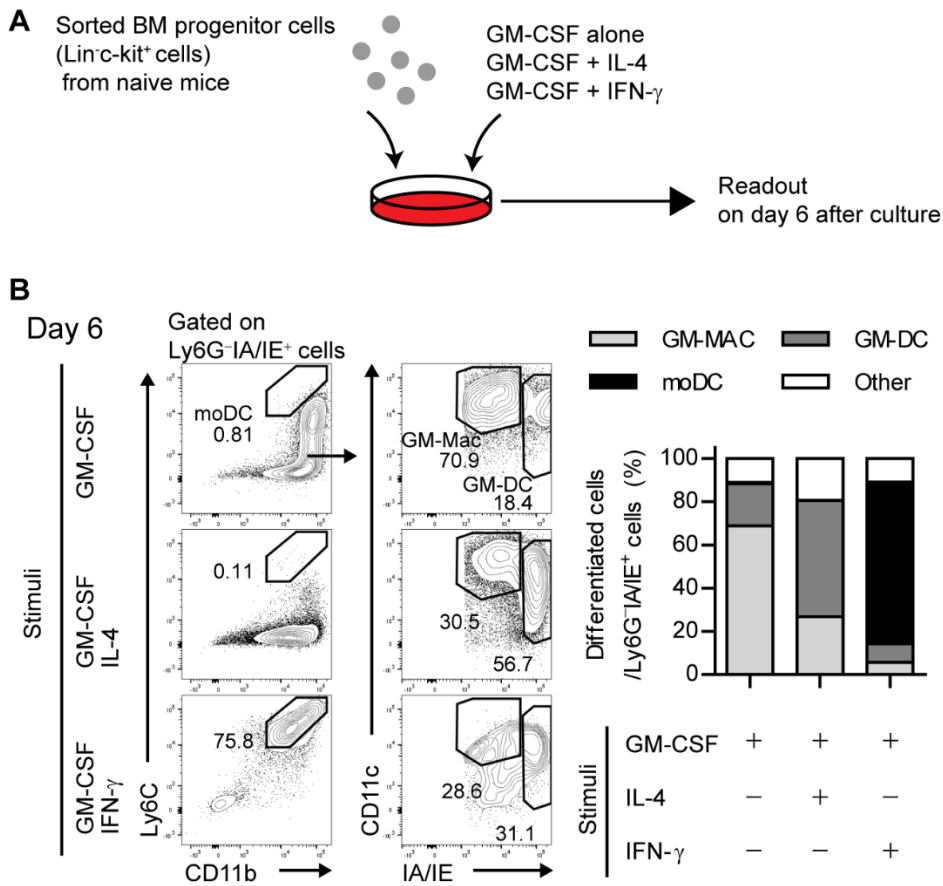

Figure 13. IFN-γ directs the differentiation of moDCs from BM progenitor cells

Lin$^-$C-kit$^+$ BM progenitor cells were sorted from naive mice and cultured under different cytokine stimulus. (**A**) Experimental schedule. (**B**) Differentiation patterns of total BMPs at day 6 under different stimulus (GM-CSF alone, GM-CSF + IL-4 and GM-CSF + IFN-γ) are shown as FACS plots (left) and graph plots (right). Numbers in FACS plots indicate the percentages of the gates.

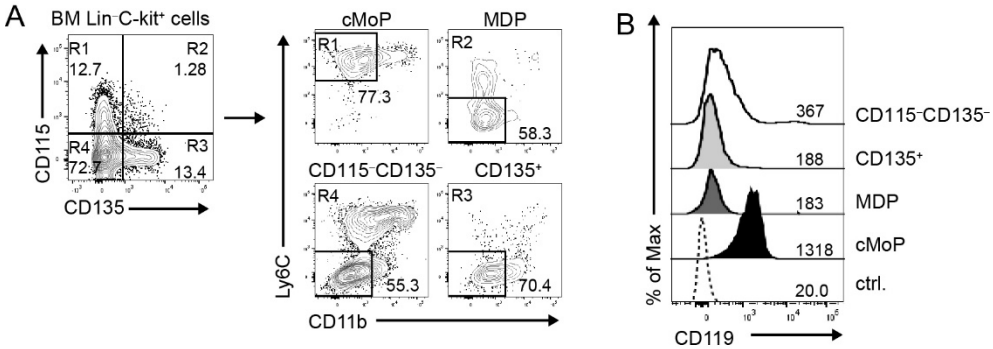

Figure 14. IFN-γR expression is selectively elevated in common monocyte progenitor cells

(A) Gating and sorting strategy for $CD115^{-}CD135^{-}$, $CD135^{+}$, MDP and cMoP in BMPs. Numbers indicate the percentages of the gates. **(B)** IFN-γR (CD119) expression levels of BMP subsets. Numbers indicate the MFI values of each subset.

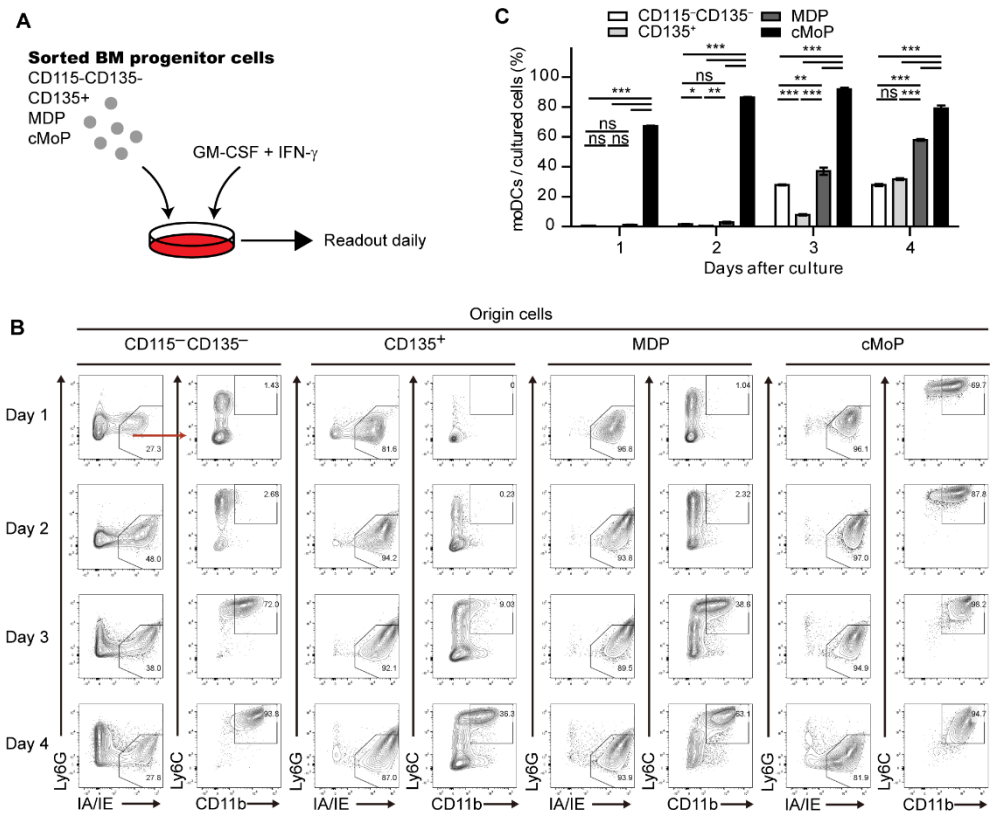

Figure 15. cMoPs directly respond to IFN-γ and differentiate into moDCs

Daily differentiation of the subdivided BMP subsets into moDCs under GM-CSF and IFN-γ stimulation. (**A**) Experimental schedule. (**B**) Flow cytometry plots of sorted BMP subsets during culture. Numbers in FACS plots indicate the percentages of the gates. (**C**) Graph shows the proportions of cells that differentiate into moDCs in each BMP subset. Data are representative of three independent experiments and are shown as the mean±SEM. *p<0.05;**p<0.01; ***p<0.001.

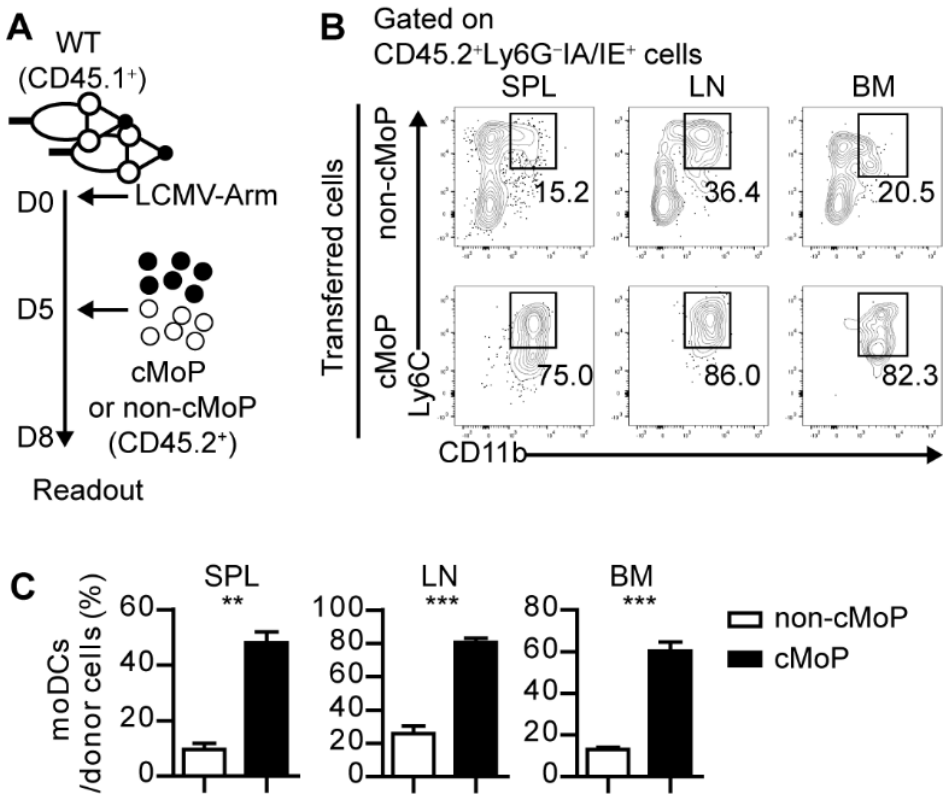

Figure 16. cMoPs immediately differentiate into moDCs in LCMV-Arm-infected mice

(A) Experimental schedule for analyzing the *in vivo* differentiation of cMoPs into moDCs during infection. **(B-C)** Differentiation of $CD45.2^+$ donor cells into moDCs in the indicated organ of LCMV-Arm infected mice are shown as FACS plots **(B)** and graph plots **(C)**. Numbers in FACS plots indicate the percentages of the gates. Data are representative of two independent experiments and are shown as the mean±SEM. **p<0.01; ***p<0.001.

III.III. $CD8^+$ T cells primed by moDCs have reduced effector function than those primed by cDCs

Given that moDCs become the dominant population of APCs during the expansion phase of acute viral infection, moDCs may be involved in modulating antiviral T cell responses. Thus, I determined whether infection-induced moDCs play an essential role in the virus-specific $CD8^+$ T cell responses. To compare the ability of each DC subset to stimulate $CD8^+$ T cell responses, I isolated moDCs and cDCs from the LCMV-Arm-infected mice on day 4 p.i. and cocultured the cells in the presence of various doses of cognate peptide (GP_{33-41}) with Cell trace violet (CTV)-labeled P14 cells, which express TCRs that recognize the epitope peptide of the LCMV glycoprotein **(Figure 17A)**. moDCs were shown to have lower priming capacity than that of cDCs under low antigenic peptide stimulation (20 ng/ml), suggesting that moDCs deliver weak signals to $CD8^+$ T cells **(Figures 17B and 17C)**. Then, I compared the surface phenotypes of the P14 cells that were primed by each DC subset. Analysis of surface marker expression levels revealed that, while CD44 expressions were comparable between the two cell types, cDC-stimulated P14 cells ($P14_{cDC}$) were more activated than moDC-stimulated P14 cells ($P14_{moDC}$) as shown by elevated CD25 (IL-2Rα) and CD69 levels. Instead, $P14_{moDC}$ showed upregulated expressions of

CD122 (IL-2/15 Rβ) and CD132 (common γ chain) compared to $P14_{cDC.}$ CD127 (IL-7R) levels were similar between $P14_{cDC}$ and $P14_{moDC,}$ and IL-15Rα was rarely detectable in both cell types **(Figure 18A)**. Interestingly, when P14 cells were plotted by their coexpressions of CD25 and CD62L, $P14_{moDC}$ displayed a predominantly memory-like phenotype ($CD25^{low}CD62L^{hi}$), whereas $P14_{cDC}$ had a higher fraction of effector-like cells ($CD25^{hi}CD62L^{low}$) **(Figure 18B)**(41, 42). Moreover, $P14_{moDC}$ showed reduced expressions of effector molecules (IFN-γ, TNF-α and granzyme B (GzmB)) compared with those of $P14_{cDC}$ **(Figure 19A)**. Similar results were obtained in the experiments using APCs isolated from infected mice on day 8 p.i. Day 8 moDCs were indistinguishable from day 4 moDCs in terms of T cell-stimulating capacity **(Figure 20)**.

To directly compare antigen-specific cytolytic function of $P14_{moDC}$ with that of $P14_{cDC}$, I cocultured each type of $CD8^+$ effector T cells with GP_{33-41}-loaded EL4 tumor cells. Consistent with the expression levels of effector molecules, $P14_{moDC}$ exhibited lower target killing ability than that of $P14_{cDC}$ **(Figures 19B and 19C)**. These data suggest that moDCs were not efficient in generation of effector $CD8^+$ T cells but had an ability to induce memory precursor $CD8^+$ T cells.

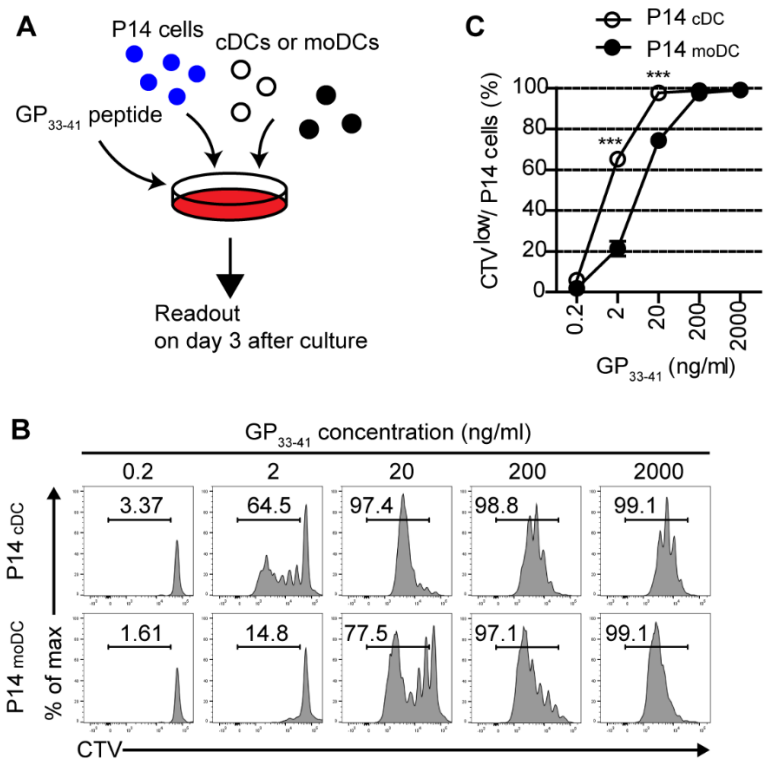

Figure 17. CD8$^+$ T cells primed by moDCs have decreased proliferative capacity

(**A**) Experimental schedule. (**B and C**) Representative histograms (**B**) and graph (**C**) of CTV dilutions in P14 cells primed by cDCs or moDCs in the presence of different doses of GP_{33-41} peptide for 3 days. Numbers in the histograms indicate the percentage of cells that were divided at least once. Data are representative of three independent experiments and are shown as the mean±SEM. ***p<0.001.

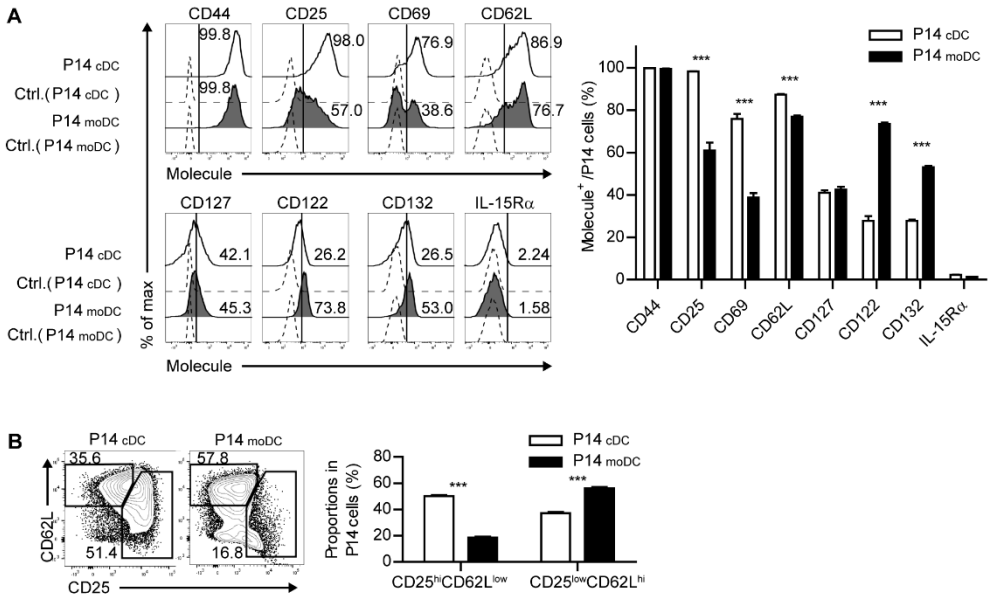

Figure 18. Surface characteristics of CD8$^+$ T cells primed by moDCs

P14 cells were stimulated as depicted in Figure 17A. (**A**) Expression levels of indicated surface molecules are shown as histograms (right) and a graph plot (left). Numbers in the histograms indicate the percentages of positive cells for each molecule. (**B**) Coexpression of CD25 and CD62L on P14 cells primed by cDCs or moDCs are shown as flow cytometry plots (left) and graph (right). Numbers in the plots indicate the percentages within each gate. Data are representative of three independent experiments and are shown as the mean±SEM. ***p<0.001.

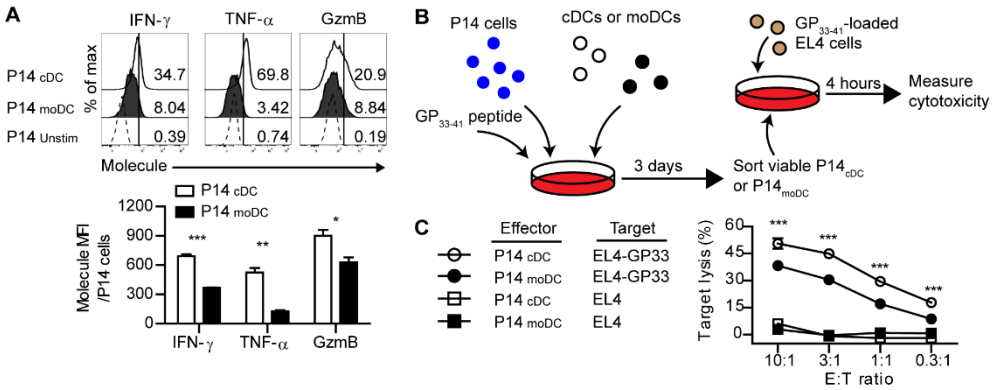

Figure 19. CD8$^+$ T cells primed by moDCs have reduced effector function than those primed by cDCs

P14 cells were stimulated as depicted in Figure 17A. (**A**) Secretion levels of the indicated effector molecules in P14 cells that were primed by cDCs or moDCs are shown as histograms (upper) and graph (lower). Numbers in the histograms indicate the percentages of positive cells for each molecule. (**B and C**) *In vitro* target killing ability of P14 cells primed by cDCs or moDCs. Cr^{51}-labeled GP_{33-41}-loaded EL4 tumor cells were used as the target cells. Experimental schedule (**B**) and graph plot (**C**). Data are representative of three independent experiments and are shown as the mean±SEM. ***p<0.001

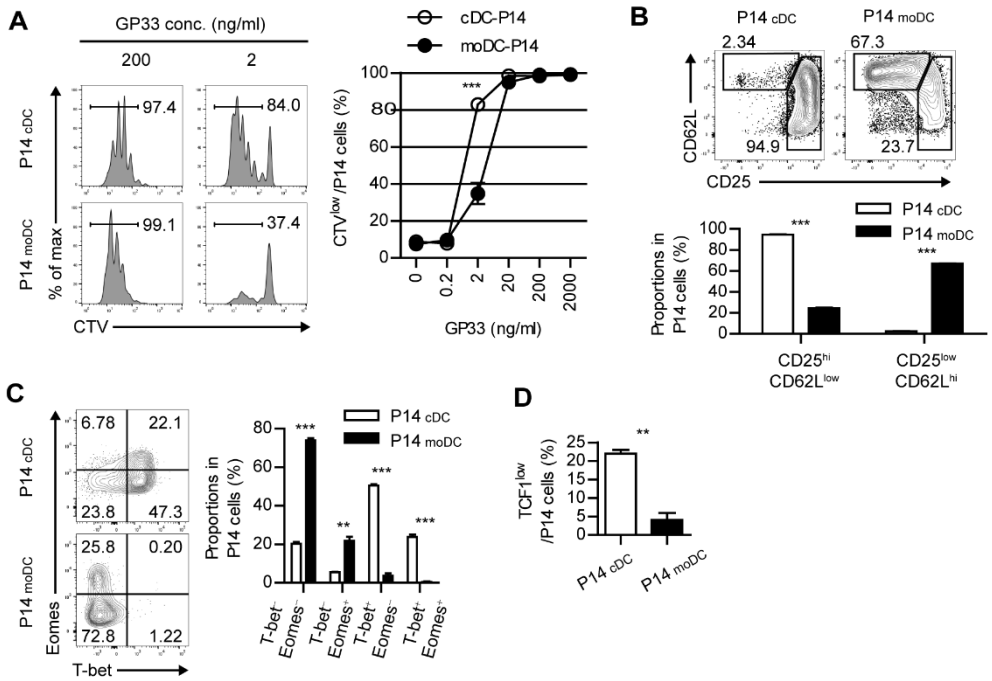

Figure 20. Differentiation patterns of P14 cells primed by moDCs that were isolated from LCMV-Arm-infected mice at day 8 p.i.

moDCs and cDCs were isolated from LCMV-Arm-infected mice at day 8 p.i. and cocultured with P14 cells in the presence of GP_{33-41} peptide for 3 days. (**A**) Dividing patterns of P14 cells primed by day 8 cDCs or moDCs are shown as histogram plots (left) and a graph plot (right). Numbers in the histogram plots indicate the percentages of divided cells in each condition. (**B**) Coexpressions of CD25 and CD62L on P14 cells primed by cDCs or moDCs are shown as flow cytometry plots (upper) and a graph plot (lower). (**C**) Coexpressions of T-bet and Eomes of P14 cells primed by day 8 cDCs or moDCs are shown as flow cytometry plots (left) and a graph plot (right). Numbers in the flow cytometry

plots indicate the percentages of each quadrant. (**D**) TCF1 expression of P14 cells primed by day 8 cDCs or moDCs is shown as a graph plot of $TCF1^{low}$ cells. Data are representative of three independent experiments and are shown as the mean±SEM. **p<0.01; ***p<0.001.

III.IV. Stimulation by moDCs dictates the developmental program of memory CD8$^+$ T cells by transcriptional regulation

It has been shown that the fate determination of CD8$^+$ T cells is regulated by the expression of several transcription factors (43). To further identify whether the signal delivered by moDCs directs CD8$^+$ T cells to memory cells, I analyzed the transcriptional changes of P14$_{cDC}$ and P14$_{moDC}$. Interestingly, P14$_{moDC}$ expressed low levels of T-bet and partly differentiated into Eomes$^+$ cells while P14$_{cDC}$ differentiated into T-bet$^+$ effector cells **(Figures 21A and 21B)**. Moreover, TCF1, a transcription factor associated with memory T cell differentiation (9), was maintained at relatively higher levels in P14$_{moDC}$ compared to that in P14$_{cDC}$ **(Figure 21A)**. The TCF1 expression level in P14$_{moDC}$ remained constant regardless of the number of cell divisions, whereas that in P14$_{cDC}$ was inversely correlated with the number of cell divisions **(Figure 21C)**. To evaluate the memory formation ability of CD8$^+$ T cells activated by moDCs, equivalent numbers of the viable P14$_{cDC}$ or P14$_{moDC}$ were transferred into LCMV-infected recipient mice on day 8 p.i. and analyzed on day 28 post transfer (day 36 p.i.) **(Figure 22A)**. The memory phenotype of P14$_{cDC}$ and P14$_{moDC}$ showed no difference at the memory time point; however, recipient mice that received

$P14_{moDC}$ had a higher number of donor cells than recipient mice that received $P14_{cDC}$, suggesting that moDCs induced long-term survival of $P14_{moDC}$ **(Figures 22B-22D)**. Overall, these results suggest that moDC stimulation diverts the fate of $CD8^+$ T cells to memory cells.

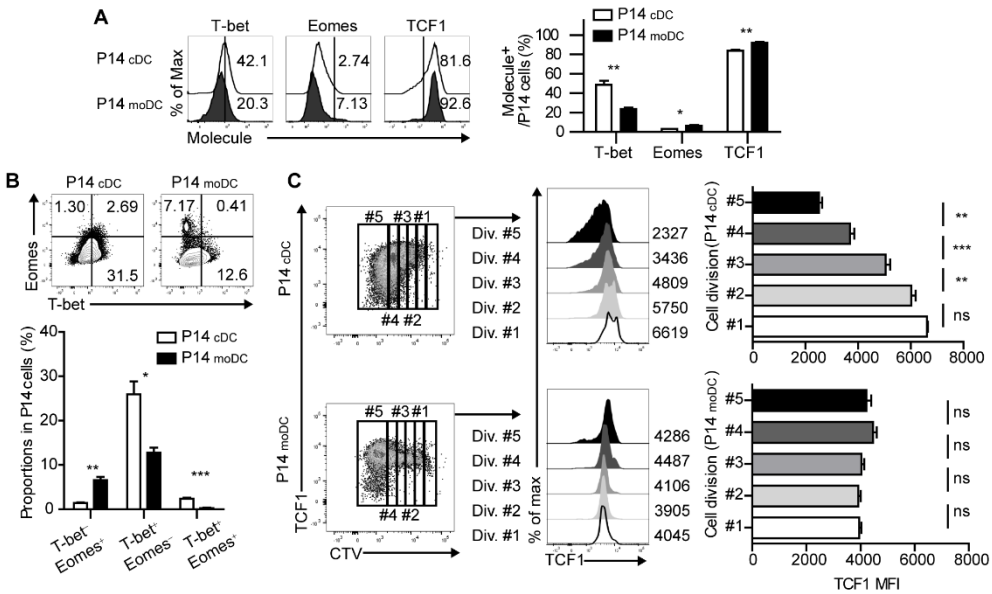

Figure 21. Stimulation by moDCs dictates the developmental program of memory CD8$^+$ T cells by transcriptional regulation

P14 cells were stimulated as depicted in Figure 17A. (**A**) Expression levels of the indicated transcription factors in P14 cells primed by cDCs or moDCs are shown as histograms (upper) and graph (lower). Numbers in the histograms indicate the percentages of positive cells for each molecule. (**B**) Coexpressions of T-bet and Eomes in P14 cells primed by cDCs or moDCs are shown as flow cytometry plots (upper) and graph (lower). Numbers in the plots indicate the percentages of the cells in each quadrant. (**C**) P14 cells primed by cDCs or moDCs were gated by their cell division (left). TCF1 expression levels of each gate are shown as histograms (center) and graphs (right). Numbers in the histograms indicate the

MFI values of TCF1 expression in each gate. Data are representative of three independent experiments and are shown as the mean±SEM. *p<0.05; **p<0.01; ***p<0.001.

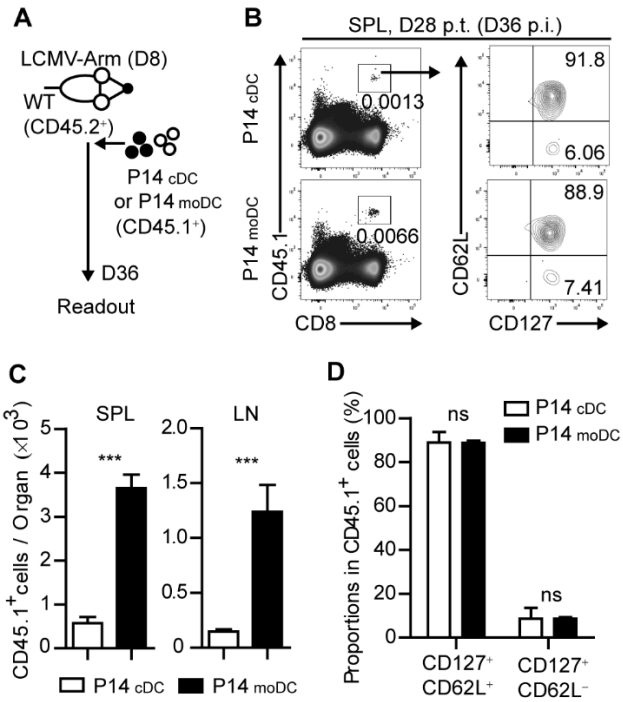

Figure 22. CD8$^+$ T cells primed by moDCs survive longer *in vivo* than those primed by cDCs

CD45.1$^+$ P14 cells were primed *in vitro* by cDCs or moDCs, transferred to infected recipient mice on day 8 p.i., and analyzed on day 28 post transfer. (**D**) Experimental schedule. (**E**) Representative flow cytometry plots of donor cells in the spleens of recipient mice. (**F**) Graphs show the number of donor P14 cells in the indicated organs. (**G**) Graphs show the coexpressions of CD127 and CD62L of the donor cells in the spleen of the recipient mice. Data are representative of two independent experiments and are shown as the mean±SEM. n=3 per group. ***p<0.001.

III.V. $CD8^+$ T cells fail to differentiate into MPECs in CCR2-deficient mice

To determine the role of moDCs in the fate determination of $CD8^+$ T cells during acute viral infection, I used CCR2-deficient (*Ccr2*$^{-/-}$) mice. While the frequency and composition of cDCs was comparable to that in the WT mice, moDCs in SLOs were dramatically reduced in the *Ccr2*$^{-/-}$ mice compared to WT mice during infection **(Figures 23A and 23B)**. The virus titers of *Ccr2*$^{-/-}$ mice and WT mice showed no differences during the acute phase of infection **(Figure 23C)**. I transferred $CD45.1^+$ P14 cells into WT and *Ccr2*$^{-/-}$ mice, which were subsequently infected with LCMV-Arm, and analyzed the transferred P14 cells on day 8 p.i. To dissect the fate of $CD8^+$ T cells, I subdivided the donor T cells by the distinct expression pattern of KLRG1 and CD127. When WT and *Ccr2*$^{-/-}$ mice bearing $CD45.1^+$ P14 cells were infected, the frequency of $KLRG1^+CD127^-$ cells, identified as short-lived effector cells (SLECs), was significantly increased in P14 cells in *Ccr2*$^{-/-}$ mice compared with that in WT mice. In addition, the frequency of $KLRG1^-CD127^+$ cells, which represent memory precursor cells (MPECs), was significantly reduced in *Ccr2*$^{-/-}$ hosts, suggesting that $CCR2^+$ cells contributed to the efficient generation of memory $CD8^+$ T cells during infection **(Figures 24A and 24B)**. I also examined the effector function of P14 cells in WT

and *Ccr2*$^{-/-}$ mice. The intensity, but not the frequency, of IFN-γ or TNF-α–producing T cells among P14 cells was elevated in *Ccr2*$^{-/-}$ mice compared with that in WT mice **(Figure 24C)**. Furthermore, P14 cells from *Ccr2*$^{-/-}$ mice showed more potent target cell killing activity than those from WT mice **(Figure 24D)**.

To determine whether the altered effector/memory differentiation of virus-specific CD8^{+} T cells in *Ccr2*$^{-/-}$ mice reflects molecular changes in CD8^{+} T cells, I compared the transcriptional profile of SLECs and MPECs in transferred P14 cells of WT and *Ccr2*$^{-/-}$ mice. Consistent with the results of the *in vitro* studies (Figure 21), the expressions of Eomes and TCF1 in each P14 cell subset were decreased in *Ccr2*$^{-/-}$ mice compared with those in WT mice and the effect was more prominent in MPECs **(Figures 25A and 25B)**. Despite the reduced numbers of moDCs, SLECs and MPECs of P14 cells in *Ccr2*$^{-/-}$ mice had low levels of T-bet expression, suggesting that other factors could have contributed to the transcriptional changes in CD8^{+} T cells. In addition, the expressions of *Tcf7* and *Eomes* in P14 cells were significantly reduced in *Ccr2*$^{-/-}$ recipient mice compared to WT mice, while the expressions of *Tbx21* and *Prdm1* were similar **(Figure 25C)**. Collectively, these results suggest that moDCs can induce memory precursor cells from naïve CD8^{+} T cells by regulation of transcription factor expression including Eomes and TCF1.

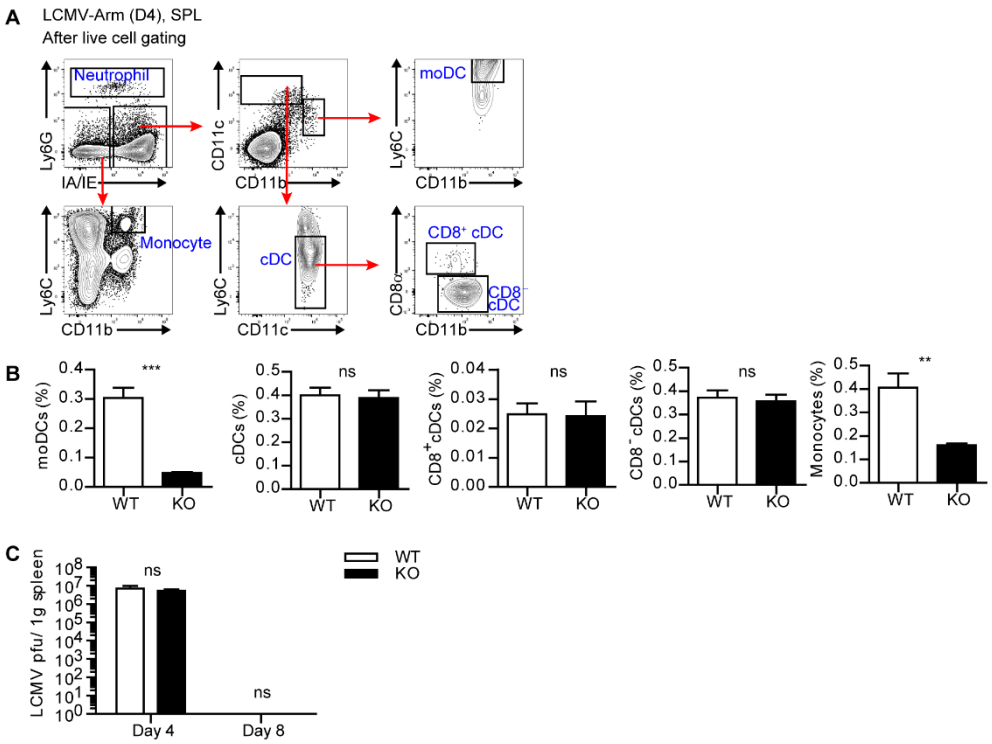

Figure 23. CCR2-deficient mice exhibit reduced numbers of moDCs and monocytes during LCMV-Arm infection

(**A**) Gating strategy for moDCs, monocytes and cDCs in the splenocytes of LCMV-Arm-infected mice 4 days p.i. (**B**) The frequencies of moDCs, cDCs and monocytes of LCMV-Arm-infected WT and *Ccr2*$^{-/-}$ mice are shown as graphs. (**C**) Viral titers in the spleen of WT and *Ccr2*$^{-/-}$ mice on day 4 and day 8 p.i. were calculated by the plaque assay. Data are representative of two independent experiments and are shown as the mean±SEM. n=5 per group. **p<0.01; ***p<0.001.

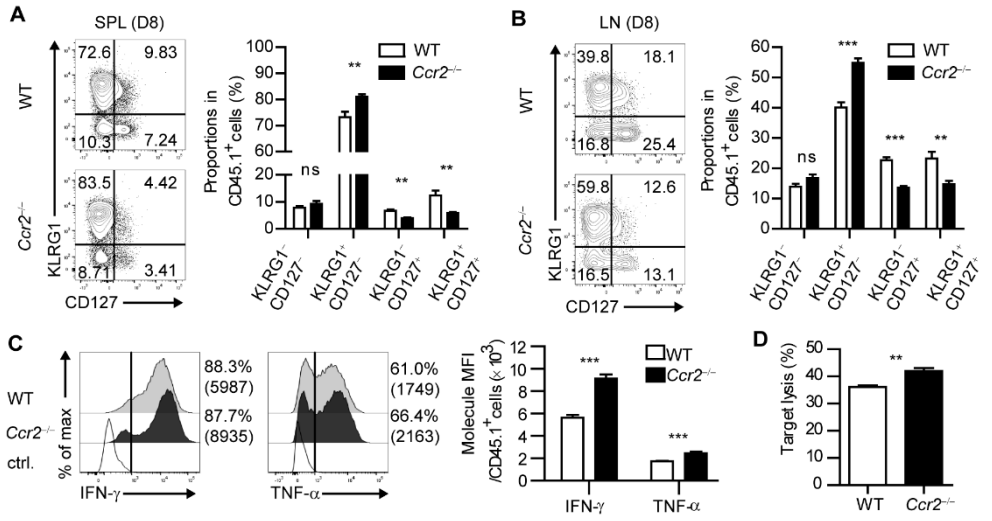

Figure 24. CD8⁺ T cells fail to differentiate into MPECs in CCR2-deficient mice

(**A and B**) Coexpressions of KLRG1 and CD127 of CD45.1⁺ P14 cells in the spleen (**A**) and LN (**B**) of LCMV-Arm-infected WT and *Ccr2*$^{-/-}$ mice on day 8 p.i. are shown as flow cytometry plots (left) and graph (right). Numbers in the plots indicate the percentage of cells within each quadrant. (**C**) Secretion levels of IFN-γ and TNF-α in CD45.1⁺ P14 cells in the spleen of WT and *Ccr2*$^{-/-}$ mice on day 8 p.i. are shown as histograms (left) and graph (right). (**D**) *In vitro* target killing ability of CD45.1⁺ P14 cells from WT and *Ccr2*$^{-/-}$ splenocytes on day 8 p.i. Cr^{51}-labeled GP_{33-41}-loaded EL4 tumor cells were used as the target cells. Data are representative of three independent experiments and are shown as the mean±SEM. n=5 per group. **p<0.01; ***p<0.001.

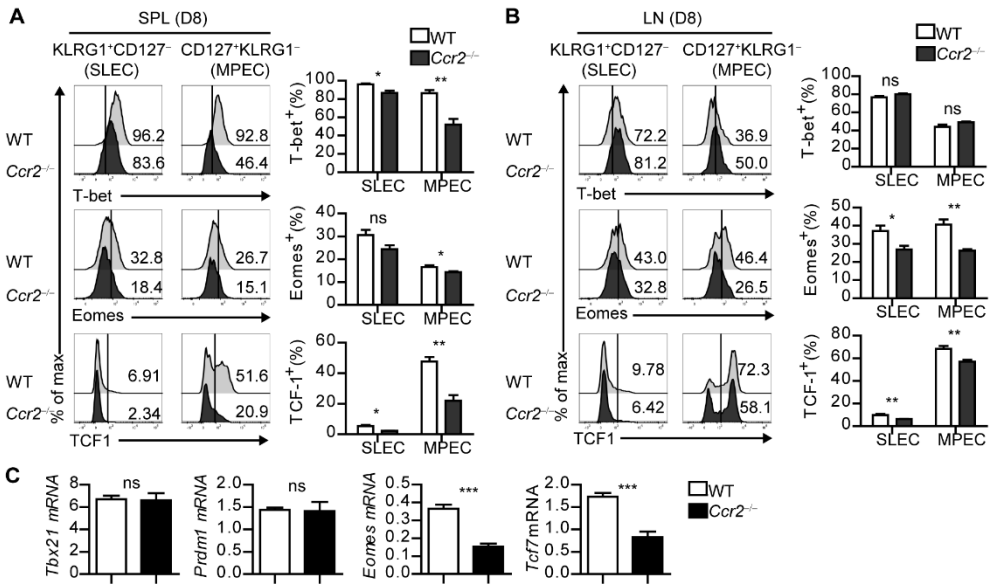

Figure 25. CD8$^+$ T cells in moDC-deficient mice undergo effector-prone differentiation

(**A and B**) Expression levels of T-bet, Eomes and TCF1 in SLECs and MPECs of CD45.1$^+$ P14 cells from WT and *Ccr2*$^{-/-}$ splenocytes (**A**) and LN cells (**B**) on day 8 p.i. are shown as histograms (upper) and graph (lower). Numbers in the histograms indicate the percentage of positive cells for each molecule. (**C**) Gene expression levels of *Tbx21*, *Prdm1*, *Eomes* and *Tcf7* in CD45.1$^+$ P14 cells from WT and *Ccr2*$^{-/-}$ splenocytes on day 8 p.i. were measured by real-time PCR. Expression levels were normalized to m*Hprt*. Data are representative of three independent experiments and are shown as the mean±SEM. n=5 per group. *p<0.05; **p<0.01; ***p<0.001.

III.VI. $CD8^+$ T cells primed in CCR2-deficient mice cannot respond to reinfection

Then, I analyzed transferred P14 cells at the memory phase of infection. On day 35 p.i., P14 cells were barely detectable in the spleen and LN of *Ccr2*$^{-/-}$ mice **(Figures 26A and 26C)**, which may be due to reduced frequencies of MPECs in *Ccr2*$^{-/-}$ mice at the early phase of infection. However, the phenotype of the remaining P14 cells in WT and *Ccr2*$^{-/-}$ mice was similar except that fraction of $CD127^-CD62L^-$ cells was slightly increased in splenic P14 cells of *Ccr2*$^{-/-}$ mice **(Figures 26B and 26D)**. Additionally, P14 memory cells in *Ccr2*$^{-/-}$ mice had similar inflammatory potency compared with those in WT mice **(Figure 26E)**. These results suggest that moDCs play a major role in maintaining the memory $CD8^+$ T cell pool without affecting their functions.

To examine whether virus-specific $CD8^+$ T cell priming by moDCs leads to enhanced protection against rechallenge, I harvested $CD45.1^+$ effector P14 cells from WT or *Ccr2*$^{-/-}$ mice on day 8 post LCMV-Arm infection. Then, I transferred an equivalent number of each type of P14 cells into naive WT recipient mice to establish LCMV-specific memory $CD8^+$ T cells in the hosts **(Figure 27A)**. As expected, P14 cells primed in WT mice preferentially survived in the hosts compared to those primed in *Ccr2*$^{-/-}$ mice, as shown by reduced numbers of

CD45.1^{+} P14 cells from *Ccr2*$^{-/-}$ mice in the blood, spleen and liver in recipient mice over 20 days post transfer, with a minor alteration in the phenotype of these cells **(Figures 27B-27D)**. I infected recipient mice with Lm-GP33 on day 26 after transfer. Consistent with the reduced memory P14 cell numbers before reinfection, mice that received effector P14 cells from *Ccr2*$^{-/-}$ mice could not control bacterial burden while mice that received P14 cells from WT mice showed reduced bacterial burden compared with the untransferred control **(Figure 27E)**. Taken together, these data suggest that moDCs induced by infection are crucial in the long-term survival of CD8^{+} T cells, thus enabling efficient clearance of pathogens by the hosts upon reinfection.

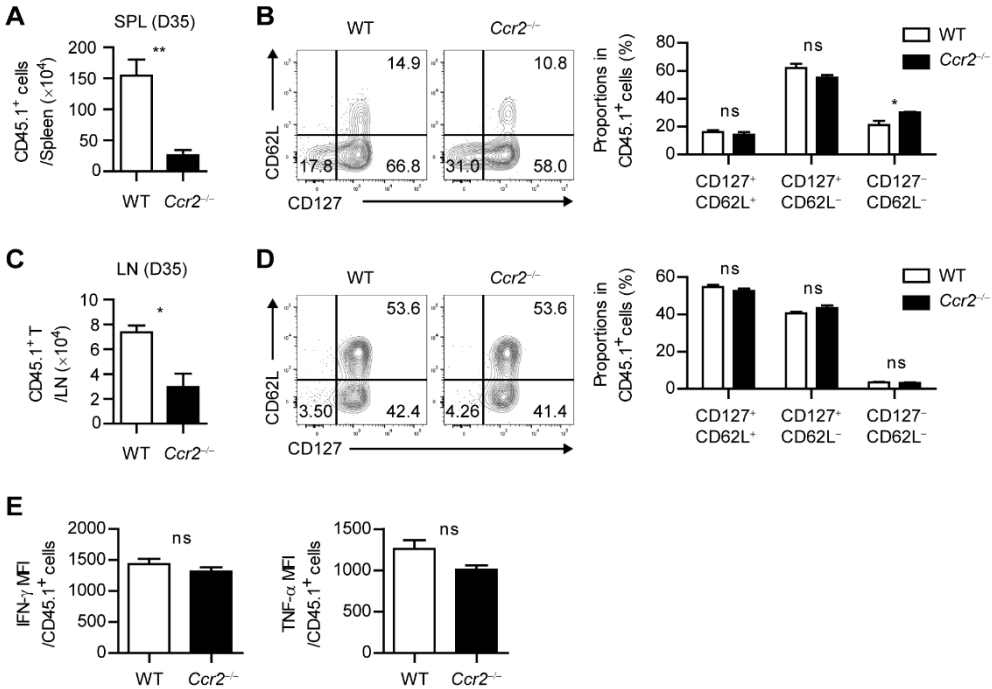

Figure 26. CCR2-deficient mice fail to generate proper CD8$^+$ T memory without affecting their quality

WT and *Ccr2*$^{-/-}$ mice containing CD45.1$^+$ P14 cells were infected with LCMV-Arm and donor P14 cells were analyzed on day 35 p.i. (**A-D**) The numbers of CD45.1$^+$ P14 cells was determined in the spleen (**A**) and LN (**C**) and the coexpression of CD62L and CD127 of CD45.1$^+$ P14 cells was analyzed in the spleen (**B**) and LN (**D**) of WT and *Ccr2*$^{-/-}$ mice. Numbers in the flow cytometry plots indicate the percentage of each quadrant. (**E**) Secretion levels of IFN-γ and TNF-α in CD45.1$^+$ P14 cells in the spleen of WT and *Ccr2*$^{-/-}$ mice are shown as

graphs. Data are representative of two independent experiments and are shown as the mean±SEM. n=3-4 per group. *$p<0.05$;**$p<0.01$.

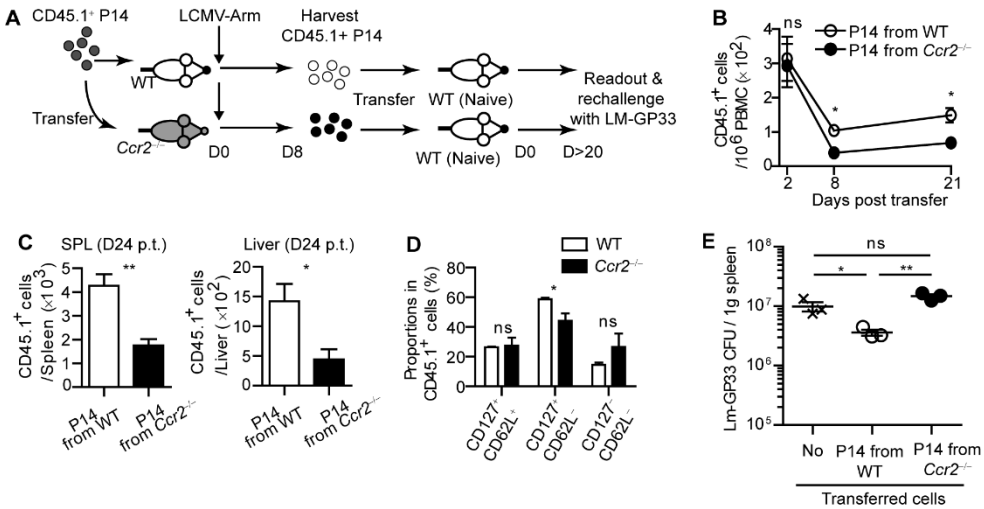

Figure 27. CD8$^+$ T cells primed in CCR2-deficient mice cannot respond to reinfection

Effector P14 cells of WT and *Ccr2*$^{-/-}$ mice at day 8 p.i. were sorted and equivalent numbers of the cells were transferred into naïve mice. Recipient mice were analyzed at least 20 days after transfer. (**A**) Experimental schedule. (**B**) Temporally enumerated CD45.1$^+$ P14 cells in blood PBMCs of recipient mice after the transfer of effector P14 cells from WT and *Ccr2*$^{-/-}$ mice. (**C**) The frequencies of CD45.1$^+$ P14 cells in the spleen (left) and liver (right) of recipient mice on day 24 post transfer of P14 cells from WT and *Ccr2*$^{-/-}$ mice. (**D**) The memory phenotypes of CD45.1$^+$ P14 cells in the spleen of recipient mice on day 24 post transfer of P14 cells from WT and *Ccr2*$^{-/-}$ mice. (**E**) Recipient mice were challenged with Lm-GP33 at day 26 post transfer. Graph shows the bacterial titers in the spleen of recipient mice at day 3 after rechallenge. Data are

representative of two independent experiments and are shown as the mean±SEM. n=3-4 per group. *$p<0.05$; **$p<0.01$.

III.VII. Defective IL-2 signaling grants moDCs an ability to induce memory CD8$^+$ T cells

Finally, I sought to investigate the underlying mechanisms that mediate the differentiation of memory-precursor cells during the interaction between CD8$^+$ T cells and moDCs. Three signals have been known to be responsible for the initial activation of CD8$^+$ T cells: TCR-MHC interaction, costimulation and cytokine signaling (1, 4). moDCs showed no defect in the expression of MHCI and costimulatory molecules (CD40, CD80 and CD86) compared to those of cDCs **(Figure 28)**. Thus, I hypothesized that defective cytokine signaling caused moDCs to deliver relatively weak signals to CD8$^+$ T cells. Interestingly, the differentiation patterns of CD8$^+$ T cells primed in the presence of a high dose of IL-2 and in the presence of a low dose of IL-2 resembled P14$_{cDC}$ and P14$_{moDC}$, respectively (44, 45). Accordingly, the levels of IL-2 in the supernatants of P14 cells cocultured with cDCs were higher than in those cocultured with moDCs **(Figure 29A)**. Moreover, only cDCs expressed IL-2 at the transcript level **(Figure 29B)**. In addition, an analysis of IL-2 secretion levels in the cocultures 12 hours after culture revealed that cDCs produced more IL-2 than moDCs and P14$_{cDC}$ expressed high levels of IL-2 compared to P14$_{moDC}$ **(Figure 30)**. Therefore, I hypothesized that defective IL-2 signaling is responsible for the

differentiation of $CD8^+$ T cells into $CD25^{low}CD62L^{hi}$ memory precursor cells.

To test this possibility, I cultured $CD8^+$ T cells with cDCs or moDCs in the presence of anti-IL-2 mAbs (αIL-2) or recombinant IL-2 (rmIL-2). In agreement with my hypothesis, $P14_{cDC}$ cells cultured with αIL-2 predominantly differentiated into $CD25^{low}CD62L^{hi}$ memory phenotype cells suggesting that IL-2 was required for the full effector cell differentiation of P14 cells **(Figures 31A and 31B)**. Due to the endogenous IL-2 secretion of $P14_{cDC}$, adding rmIL-2 to cocultures showed no effect on the surface phenotypes of $P14_{cDC}$. $P14_{moDC}$, which were mainly differentiated into $CD25^{low}CD62L^{hi}$ memory precursor cells, were converted into $CD25^{hi}CD62L^{low}$ effector cells by adding rmIL-2 to the cocultures. I also found that the culture of $P14_{cDC}$ with αIL-2 abrogated the downregulation of TCF1, whereas the culture of $P14_{moDC}$ with rmIL-2 showed dramatic suppression of TCF1 expression **(Figures 31C and 31D)**. Collectively, these results suggest that IL-2 signaling is important for modulation of the fate of $CD8^+$ T cells during priming and that moDCs promote memory-prone differentiation of $CD8^+$ T cells by delivering defective signaling such as IL-2.

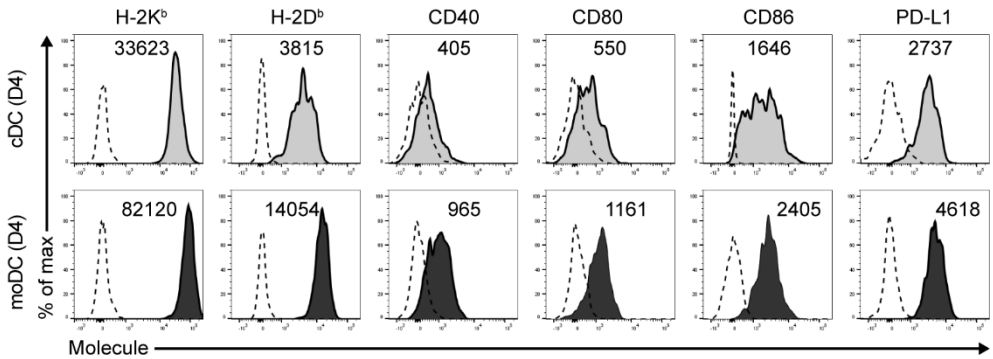

Figure 28. Expression levels of surface molecules involved in T cell signaling of cDCs and moDCs

The expression levels of MHCI (H-2K^b and H-2D^b), costimulatory (CD40, CD80 and CD86) and coinhibitory (PD-L1) molecules of cDCs and moDCs from LCMV-Arm infected mice at day 4 p.i. were measured by flow cytometry and are shown as histograms. Numbers in the histograms indicate the MFI values of each molecule. Dashed histograms indicate isotype Ab staining.

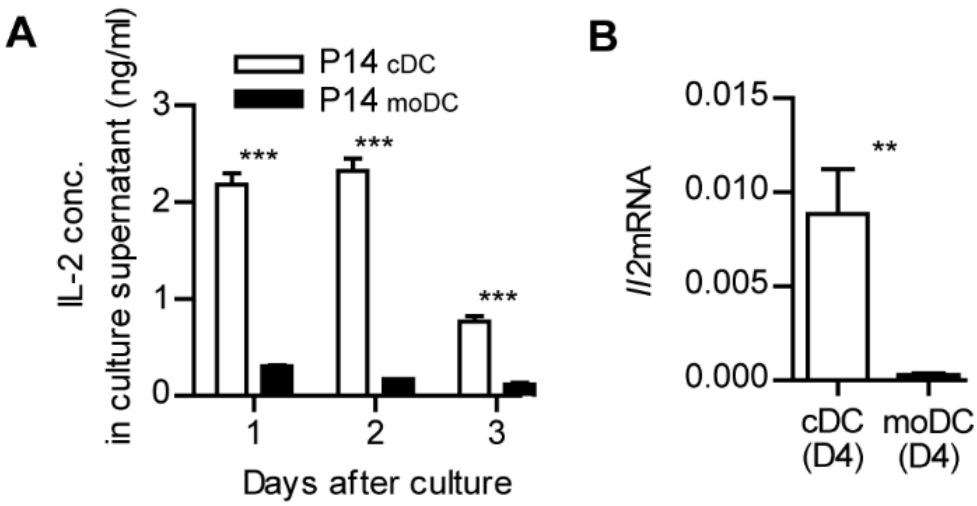

Figure 29. IL-2 production is defective in cocultures of CD8$^+$ T cells and moDCs

(A) IL-2 concentrations in the supernatant from cultures of P14 cells with cDCs or moDCs. **(B)** Gene expression levels of *Il2* in cDCs and moDCs isolated from LCMV-Arm infected splenocytes at day 4 p.i.

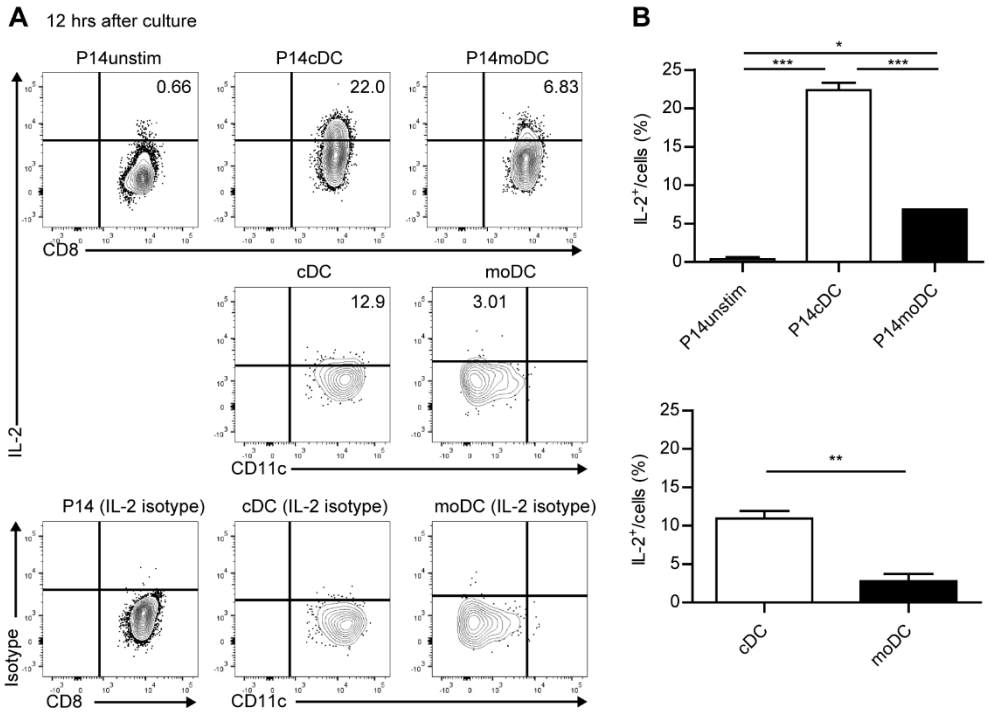

Figure 30. IL-2 secretion levels of T cells and DCs in the early time point of cocultures

moDCs and cDCs isolated from LCMV-Arm-infected mice were cocultured with P14 cells in the presence of GP_{33-41} peptide, and IL-2 secretion levels of P14 cells and of each DC subset were determined by intracellular cytokine staining at 12 hours after culture. GolgiPlug were added to culture 4 hours prior to analysis. (**A**) Representative flow cytometry plots. Numbers in the plots indicate the IL-2^+ percentages of indicated subsets. (**B**) Graph plots of IL-2^+ cells within each T cell and DC subset. Data are shown as the mean±SEM. *p<0.05;**p<0.01;***p<0.001.

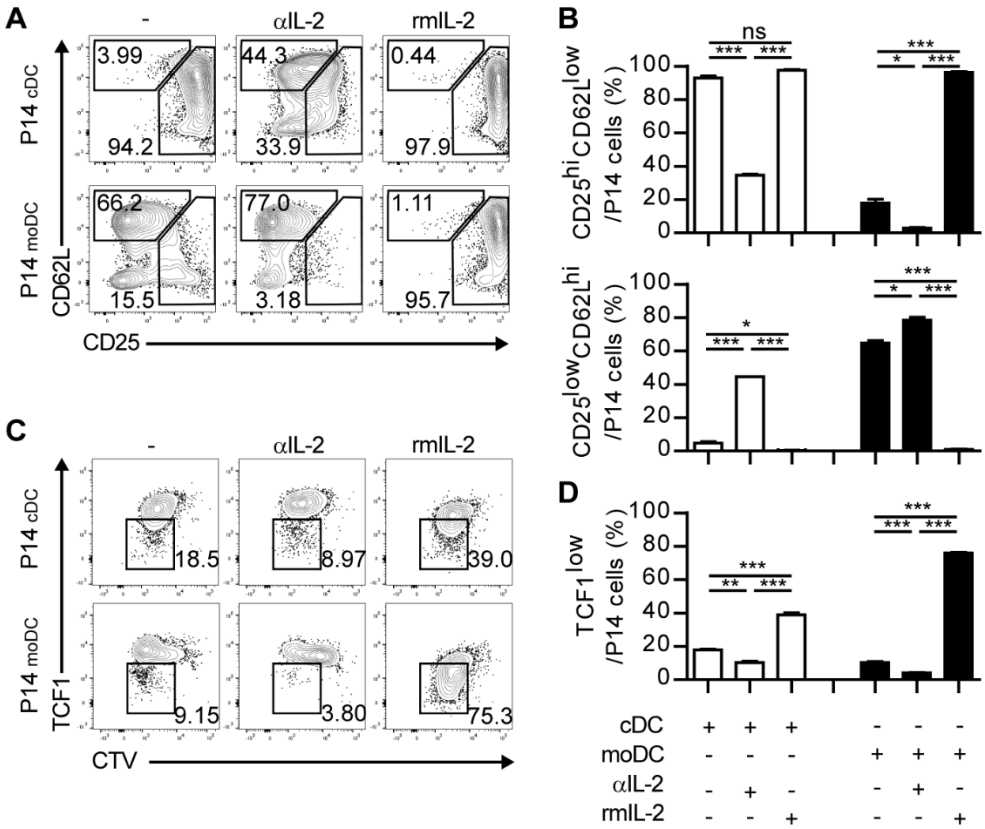

Figure 31. Defective IL-2 signaling grants moDCs an ability to induce memory CD8$^+$ T cells

Recombinant IL-2 or anti-IL-2 mAbs were added to the cultures of P14 cells with moDCs or cDCs. (**A and B**) Coexpressions of CD25 and CD62L under each condition are shown as flow cytometry plots (**A**) and graphs (**B**). (**C and D**) Expression levels of TCF1 are shown as flow cytometry plots (**C**) and graph (**D**). Numbers in the plots indicate the percentage within each gate. Data are representative of two independent experiments and are shown as the mean±SEM. *p<0.05; **p<0.01; ***p<0.001.

IV. Discussion

Understanding the mechanism of the influence of myeloid cells on the development of T cell immunity during infection is important for establishing strategies for development of vaccines against infections. Here, I demonstrate that moDCs dramatically expand in an IFN-γ dependent manner during acute infection. More importantly, $CD8^+$ T cells activated by moDCs preferentially differentiate to memory cells by inducing Eomes expression and maintaining TCF1 expression, while those cells that are primed by cDCs undergo effector-prone differentiation through upregulation of T-bet and downregulation of TCF1. Moreover, I found that the difference in IL-2 production between the two APC subsets results in the different outcomes of the primed $CD8^+$ T cells **(Figure 32)**.

APC subsets with distinct properties have been proposed to be crucial for the differentiation of T cells (34, 46). My study suggests that the interaction between T cells and distinct APC subsets during priming regulates the fate of $CD8^+$ T cells. Since cDCs are enriched in the SLOs during the initial phase of acute viral infection, they may serve as the primary professional APCs that prime $CD8^+$ T cells resulting in the predominant generation of effector T cells. As the increased effector $CD8^+$ T cell populations primed by cDCs clear the pathogen by

producing effector molecules including IFN-γ, the elevated IFN-γ also contributes to the accumulation of moDCs in the SLOs. As a result, moDCs become abundant in the SLOs during the expansion phases of infection. It has been suggested that decreased TCR stimulation strength due to the reduced antigen burden after pathogen clearance results in the differentiation of memory $CD8^+$ T cells (3, 43); however, the data in the present study suggest another possibility that changes in the APC subset composition also contribute to the effector/memory fate determination of $CD8^+$ T cells. These data also revealed that, in addition to its direct effect on effector $CD8^+$ T cell expansion (47), IFN-γ can also influence memory $CD8^+$ T cell generation indirectly by inducing moDCs. In line with this notion, generation of memory $CD8^+$ T cell was abrogated in IFN-γR-deficient mice (48, 49). Therefore, I suggest that the changes in APC composition as well as the environment, including antigen abundance and CD4 T cell help, contribute to memory $CD8^+$ T cell formation (50).

Previous studies have shown that IFN-γ induces the differentiation of moDCs by influencing cMoPs (24, 25, 51). I confirmed this finding and found that IFN-γ potentiated moDC differentiation by directly acting on cMoPs. Although granulocyte-macrophage progenitor cells (GMPs) are known to express IFN-γR

(52), I extended this finding by showing that IFN-γR^{hi} cMoPs were the major precursor for moDC. A previous study has demonstrated that IFN-γ provokes the expansion of myeloid cells through an indirect pathway (20). I found an additional pathway by which IFN-γ induces the expansion of monocyte-derived cells, such as moDCs, via direct action on cMoPs. It is tempting to investigate why and how cMoPs selectively upregulate CD119 expression during monopoiesis.

Among the different signals that regulate the fate of CD8$^+$ T cells, defective IL-2 signaling in the cocultures of moDCs and CD8$^+$ T cells was shown to lead the memory-prone differentiation of CD8$^+$ T cells. It has been suggested that the fates of CD8$^+$ T cells are regulated by the differential exposures to IL-2 signals (53). Indeed, IL-2 signaling has been known to induce the terminal differentiation of CD8$^+$ T cells by activating STAT-5 and consequently abrogate the memory CD8$^+$ T cell generation (54). IL-2 intracellular cytokine staining showed that P14 T cells expressed higher levels of IL-2 than DCs in the cocultures, suggesting that CD8$^+$ T cells were the main source of IL-2 in the cocultures **(Figure 30)**. In addition, I found that P14$_{cDC}$ secreted more IL-2 than P14$_{moDC}$. It leads to the question of why CD8$^+$ T cells primed by cDCs secrete higher levels of IL-2 than those primed by moDCs. Interestingly, previous

studies reported that the IL-2 production by DCs allows them to stimulate T cells. DC-derived IL-2 accumulation at the DC-T contact site has been considered to be important in the stimulation of T cells (55-57). From the viewpoint of these findings, my data suggest that cDCs, potent IL-2 providers, induce robust IL-2 production from $CD8^+$ T cells and dictate terminal differentiation of $CD8^+$ T cells. On the other hand, moDCs stimulate $CD8^+$ T cells suboptimally via attenuated IL-2 signaling and promote the differentiation of memory-phenotype cells. In summary, DCs are likely to contribute to the fate determination of $CD8^+$ T cells by regulating IL-2 signaling, especially at the initial priming phase.

Long-term survival of memory $CD8^+$ T cells is mediated by homeostatic proliferation (58). *In vitro* coculture analysis revealed that $P14_{moDC}$ expressed high levels of CD122 and CD132, which are the subunits of IL-15 receptor, compared to $P14_{cDC}$. As IL-15 plays an important role in maintaining memory T cells (59, 60), it might have been involved in the long-term survival of $P14_{moDC}$ when $P14_{moDC}$ were adoptively transferred to mice. Although IL-15Rα was not detected in $P14_{moDC,}$ other IL-15Rα–expressing cells could have delivered IL-15 signaling to $P14_{moDC}$ via trans-presentation(61). Thus, I suggest that moDCs direct $CD8^+$ T cells to express IL-15 receptors, enabling $CD8^+$ T cells to survive at the memory phase.

The mechanisms for effector/memory differentiation of $CD8^+$ T cells have been incompletely understood. Asymmetric cell division, which directs proximal and distal daughter cells to differentiate into SLECs and MPECs, respectively, has recently emerged as one of the mechanisms explaining how effector and memory progenies occur from naïve parental T cells (42, 62). A previous report suggested that strong TCR stimulation is required for the initiation of asymmetric cell division of $CD8^+$ T cells. On the contrary, weak TCR stimulation preferentially leads to symmetric cell division of $CD8^+$ T cells, resulting in the increased generation of MPECs(63). These results suggest that different TCR stimulation capacity of each DC subset could determine the fate of $CD8^+$ T cells through differential regulation of the symmetry of cell division. In this regard, it would be interesting to compare the asymmetry in T cell division upon stimulation with different DC subsets.

I used *Ccr2*$^{-/-}$ mice to define the roles of moDCs in $CD8^+$ T cell differentiation during infection *in vivo*. The reduced memory $CD8^+$ T cell responses in *Ccr2*$^{-/-}$ mice correlated with *in vitro* studies that demonstrated the specialized role of moDCs in the induction of memory precursor cells. I were unable to rule out the contribution of monocytes to memory $CD8^+$ T cell differentiation because *Ccr2*$^{-/-}$ mice exhibited a decreased frequency not only of moDCs but also of monocytes

(Figure 23B). However, monocytes themselves have been considered as less efficient APCs in $CD8^+$ T cell stimulation (64). Monocytes can uptake foreign antigens, but they present antigens to T cells after subsequent differentiation into moDCs (65). Although a recent report have suggested that $Ly6C^+$ monocytes can prime $CD8^+$ T cells efficiently, a majority of $Ly6C^+CD11b^+$ cells in that report showed the feature of moDCs that express a certain level of CD11c (66). Thus, I suggest that reduction in moDCs is mainly responsible for defective memory $CD8^+$ T cell formation in *Ccr2*$^{-/-}$ mice.

It should be noted that the role of monocyte-derived cells in establishing defense mechanisms against pathogens is context-dependent. A previous report demonstrated that Tip-DCs, which share many phenotypic characteristics with moDCs in my experimental setting, mediate innate immune responses but are dispensable for T cell priming in Lm infection (23). I also showed that $CD8^+$ T cells primed in *Ccr2*$^{-/-}$ mice exhibited no defects in their cytokine production capacity and cytotoxicity during LCMV-Arm infection. However, I identified an unrecognized role of moDCs in triggering memory $CD8^+$ T cell generation under cognate antigenic stimulation. Interestingly, during the late phase of LCMV chronic (CL-13) infection, monocytes have been shown to acquire a myeloid-derived suppressor cell (MDSC)-like feature that abrogates $CD8^+$ T cell

proliferation and drives T cell exhaustion (33). The underlying factors that educate monocytic cells to play opposing roles during acute and chronic infections remain to be elucidated.

Taken together, this study demonstrates a crucial role of moDCs in the generation of memory $CD8^+$ T cells during acute antiviral immune responses. These findings expand the understanding of the link between myelopoiesis and $CD8^+$ T cell differentiation during acute viral infection and have implications for the development of novel vaccine strategies against infection.

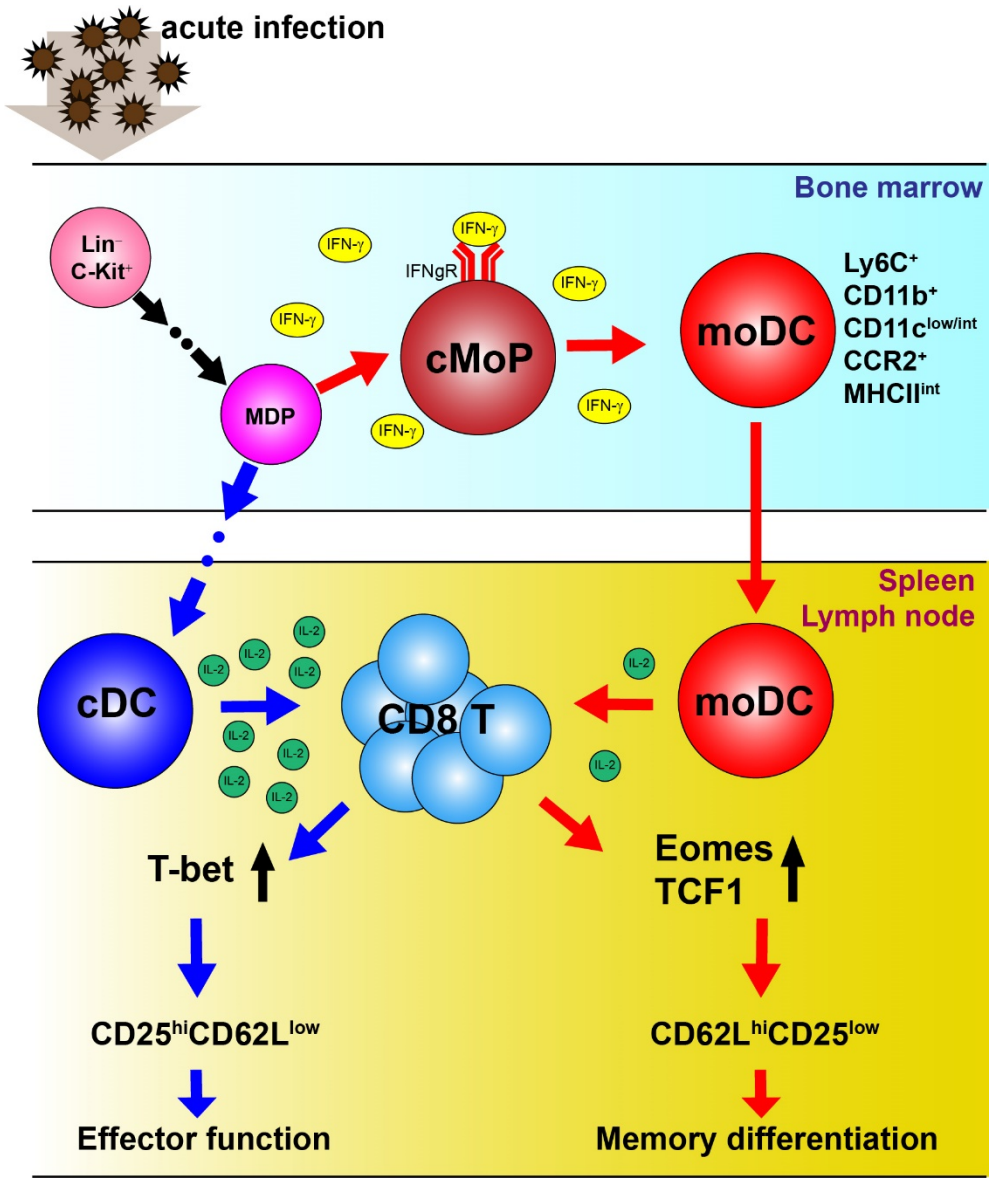

Figure 32. Graphical summary of this study

Upon acute infection, common monocyte progenitor cells (cMoPs) in the bone marrow differentiate into moDCs in an IFN-γ-dependent manner. Upregulation of IFN-γR expression level in cMoPs enables cMoPs to respond to IFN-γ directly. Differentiated moDCs are accumulated in secondary lymphoid organs such as

spleen and lymph nodes during the T cell expansion phase of infection. While cDCs prime $CD8^+$ T cells to undergo effector-prone differention through upregulation of T-bet expression, moDCs dictate memory-like differentiation of $CD8^+$ T cells by upregulation of Eomes and TCF1. As a result, $CD8^+$ T cells primed by cDCs have a potent cytotoxicity and effector functionality, whereas those primed by moDCs function as memory cells and survive for long in the host. Mechanistically, attenuated IL-2 signaling in $CD8^+$ T cells primed by moDCs is responsible for the enhanced memory programming of $CD8^+$ T cells.

V. References

1. Haring JS, Badovinac VP, Harty JT. Inflaming the CD8+ T cell response. *Immunity* (2006) 25(1):19-29. doi: 10.1016/j.immuni.2006.07.001. PubMed PMID: 16860754.

2. Joshi NS, Cui W, Chandele A, Lee HK, Urso DR, Hagman J, et al. Inflammation directs memory precursor and short-lived effector CD8(+) T cell fates via the graded expression of T-bet transcription factor. *Immunity* (2007) 27(2):281-95. doi: 10.1016/j.immuni.2007.07.010. PubMed PMID: 17723218; PubMed Central PMCID: PMCPMC2034442.

3. Chang JT, Wherry EJ, Goldrath AW. Molecular regulation of effector and memory T cell differentiation. *Nat Immunol* (2014) 15(12):1104-15. doi: 10.1038/ni.3031. PubMed PMID: 25396352; PubMed Central PMCID: PMCPMC4386685.

4. Mescher MF, Curtsinger JM, Agarwal P, Casey KA, Gerner M, Hammerbeck CD, et al. Signals required for programming effector and memory development by CD8+ T cells. *Immunological Reviews* (2006) 211(1):81-92. doi: doi:10.1111/j.0105-2896.2006.00382.x.

5. Williams MA, Bevan MJ. Effector and memory CTL differentiation. *Annu Rev Immunol* (2007) 25:171-92. doi:

10.1146/annurev.immunol.25.022106.141548. PubMed PMID: 17129182.

6. Sallusto F, Geginat J, Lanzavecchia A. Central memory and effector memory T cell subsets: function, generation, and maintenance. *Annu Rev Immunol* (2004) 22:745-63. doi: 10.1146/annurev.immunol.22.012703.104702. PubMed PMID: 15032595.

7. Kallies A, Xin A, Belz GT, Nutt SL. Blimp-1 transcription factor is required for the differentiation of effector CD8(+) T cells and memory responses. *Immunity* (2009) 31(2):283-95. doi: 10.1016/j.immuni.2009.06.021. PubMed PMID: 19664942.

8. Banerjee A, Gordon SM, Intlekofer AM, Paley MA, Mooney EC, Lindsten T, et al. Cutting edge: The transcription factor eomesodermin enables CD8+ T cells to compete for the memory cell niche. *J Immunol* (2010) 185(9):4988-92. doi: 10.4049/jimmunol.1002042. PubMed PMID: 20935204; PubMed Central PMCID: PMCPMC2975552.

9. Zhou X, Yu S, Zhao DM, Harty JT, Badovinac VP, Xue HH. Differentiation and persistence of memory CD8(+) T cells depend on T cell factor 1. *Immunity* (2010) 33(2):229-40. doi: 10.1016/j.immuni.2010.08.002. PubMed PMID: 20727791; PubMed Central PMCID: PMCPMC2928475.

10. Lefrançois L, Obar JJ. Once a killer, always a killer: from cytotoxic T

cell to memory cell. *Immunological Reviews* (2010) 235(1):206-18. doi: 10.1111/j.0105-2896.2010.00895.x.

11. Kolumam GA, Thomas S, Thompson LJ, Sprent J, Murali-Krishna K. Type I interferons act directly on CD8 T cells to allow clonal expansion and memory formation in response to viral infection. *J Exp Med* (2005) 202(5):637-50. doi: 10.1084/jem.20050821. PubMed PMID: 16129706; PubMed Central PMCID: PMCPMC2212878.

12. Obar JJ, Molloy MJ, Jellison ER, Stoklasek TA, Zhang W, Usherwood EJ, et al. CD4+ T cell regulation of CD25 expression controls development of short-lived effector CD8+ T cells in primary and secondary responses. *Proc Natl Acad Sci U S A* (2010) 107(1):193-8. doi: 10.1073/pnas.0909945107. PubMed PMID: 19966302; PubMed Central PMCID: PMCPMC2806751.

13. Sanjabi S, Mosaheb MM, Flavell RA. Opposing effects of TGF-beta and IL-15 cytokines control the number of short-lived effector CD8+ T cells. *Immunity* (2009) 31(1):131-44. doi: 10.1016/j.immuni.2009.04.020. PubMed PMID: 19604492; PubMed Central PMCID: PMCPMC2765785.

14. Boettcher S, Manz MG. Regulation of Inflammation- and Infection-Driven Hematopoiesis. *Trends Immunol* (2017) 38(5):345-57. doi: 10.1016/j.it.2017.01.004. PubMed PMID: 28216309.

15. Glatman Zaretsky A, Engiles JB, Hunter CA. Infection-induced changes in hematopoiesis. *J Immunol* (2014) 192(1):27-33. doi: 10.4049/jimmunol.1302061. PubMed PMID: 24363432; PubMed Central PMCID: PMCPMC3874119.

16. Hume DA. The mononuclear phagocyte system. *Curr Opin Immunol* (2006) 18(1):49-53. doi: 10.1016/j.coi.2005.11.008. PubMed PMID: 16338128.

17. Guilliams M, Ginhoux F, Jakubzick C, Naik SH, Onai N, Schraml BU, et al. Dendritic cells, monocytes and macrophages: a unified nomenclature based on ontogeny. *Nat Rev Immunol* (2014) 14(8):571-8. doi: 10.1038/nri3712. PubMed PMID: 25033907; PubMed Central PMCID: PMCPMC4638219.

18. Ginhoux F, Jung S. Monocytes and macrophages: developmental pathways and tissue homeostasis. *Nat Rev Immunol* (2014) 14(6):392-404. doi: 10.1038/nri3671. PubMed PMID: 24854589.

19. Jakubzick CV, Randolph GJ, Henson PM. Monocyte differentiation and antigen-presenting functions. *Nat Rev Immunol* (2017) 17(6):349-62. doi: 10.1038/nri.2017.28. PubMed PMID: 28436425.

20. Schurch CM, Riether C, Ochsenbein AF. Cytotoxic CD8+ T cells stimulate hematopoietic progenitors by promoting cytokine release from bone marrow mesenchymal stromal cells. *Cell Stem Cell* (2014) 14(4):460-72. doi:

10.1016/j.stem.2014.01.002. PubMed PMID: 24561082.

21. Shi C, Pamer EG. Monocyte recruitment during infection and inflammation. *Nat Rev Immunol* (2011) 11(11):762-74. doi: 10.1038/nri3070. PubMed PMID: 21984070; PubMed Central PMCID: PMCPMC3947780.

22. Schlitzer A, McGovern N, Ginhoux F. Dendritic cells and monocyte-derived cells: Two complementary and integrated functional systems. *Semin Cell Dev Biol* (2015) 41:9-22. doi: 10.1016/j.semcdb.2015.03.011. PubMed PMID: 25957517.

23. Serbina NV, Salazar-Mather TP, Biron CA, Kuziel WA, Pamer EG. TNF/iNOS-Producing Dendritic Cells Mediate Innate Immune Defense against Bacterial Infection. *Immunity* (2003) 19(1):59-70. doi: 10.1016/s1074-7613(03)00171-7.

24. Askenase MH, Han SJ, Byrd AL, Morais da Fonseca D, Bouladoux N, Wilhelm C, et al. Bone-Marrow-Resident NK Cells Prime Monocytes for Regulatory Function during Infection. *Immunity* (2015) 42(6):1130-42. doi: 10.1016/j.immuni.2015.05.011. PubMed PMID: 26070484; PubMed Central PMCID: PMCPMC4472558.

25. Sharma MD, Rodriguez PC, Koehn BH, Baban B, Cui Y, Guo G, et al. Activation of p53 in Immature Myeloid Precursor Cells Controls Differentiation

into Ly6c(+)CD103(+) Monocytic Antigen-Presenting Cells in Tumors. *Immunity* (2018) 48(1):91-106 e6. doi: 10.1016/j.immuni.2017.12.014. PubMed PMID: 29343444; PubMed Central PMCID: PMCPMC6005382.

26. Leon B, Lopez-Bravo M, Ardavin C. Monocyte-derived dendritic cells formed at the infection site control the induction of protective T helper 1 responses against Leishmania. *Immunity* (2007) 26(4):519-31. doi: 10.1016/j.immuni.2007.01.017. PubMed PMID: 17412618.

27. Iijima N, Mattei LM, Iwasaki A. Recruited inflammatory monocytes stimulate antiviral Th1 immunity in infected tissue. *Proceedings of the National Academy of Sciences of the United States of America* (2011) 108(1):284-9. doi: 10.1073/pnas.1005201108. PubMed PMID: PMC3017177.

28. Nakano H, Lin KL, Yanagita M, Charbonneau C, Cook DN, Kakiuchi T, et al. Blood-derived inflammatory dendritic cells in lymph nodes stimulate acute T helper type 1 immune responses. *Nat Immunol* (2009) 10(4):394-402. doi: 10.1038/ni.1707. PubMed PMID: 19252492; PubMed Central PMCID: PMCPMC2668134.

29. Chow KV, Lew AM, Sutherland RM, Zhan Y. Monocyte-Derived Dendritic Cells Promote Th Polarization, whereas Conventional Dendritic Cells Promote Th Proliferation. *J Immunol* (2016) 196(2):624-36. doi:

10.4049/jimmunol.1501202. PubMed PMID: 26663720.

30. Plantinga M, Guilliams M, Vanheerswynghels M, Deswarte K, Branco-Madeira F, Toussaint W, et al. Conventional and monocyte-derived CD11b(+) dendritic cells initiate and maintain T helper 2 cell-mediated immunity to house dust mite allergen. *Immunity* (2013) 38(2):322-35. doi: 10.1016/j.immuni.2012.10.016. PubMed PMID: 23352232.

31. Ko HJ, Brady JL, Ryg-Cornejo V, Hansen DS, Vremec D, Shortman K, et al. GM-CSF-responsive monocyte-derived dendritic cells are pivotal in Th17 pathogenesis. *J Immunol* (2014) 192(5):2202-9. doi: 10.4049/jimmunol.1302040. PubMed PMID: 24489100.

32. Augier S, Ciucci T, Luci C, Carle GF, Blin-Wakkach C, Wakkach A. Inflammatory blood monocytes contribute to tumor development and represent a privileged target to improve host immunosurveillance. *J Immunol* (2010) 185(12):7165-73. doi: 10.4049/jimmunol.0902583. PubMed PMID: 21078911.

33. Norris BA, Uebelhoer LS, Nakaya HI, Price AA, Grakoui A, Pulendran B. Chronic but not acute virus infection induces sustained expansion of myeloid suppressor cell numbers that inhibit viral-specific T cell immunity. *Immunity* (2013) 38(2):309-21. doi: 10.1016/j.immuni.2012.10.022. PubMed PMID: 23438822; PubMed Central PMCID: PMCPMC3869405.

34. Kim TS, Gorski SA, Hahn S, Murphy KM, Braciale TJ. Distinct dendritic cell subsets dictate the fate decision between effector and memory CD8(+) T cell differentiation by a CD24-dependent mechanism. *Immunity* (2014) 40(3):400-13. doi: 10.1016/j.immuni.2014.02.004. PubMed PMID: 24631155; PubMed Central PMCID: PMCPMC4017923.

35. Ban YH, Oh S-C, Seo S-H, Kim S-M, Choi I-P, Greenberg PD, et al. miR-150-Mediated Foxo1 Regulation Programs CD8+ T Cell Differentiation. *Cell Reports* (2017) 20(11):2598-611. doi: https://doi.org/10.1016/j.celrep.2017.08.065.

36. MacNamara KC, Oduro K, Martin O, Jones DD, McLaughlin M, Choi K, et al. Infection-induced myelopoiesis during intracellular bacterial infection is critically dependent upon IFN-gamma signaling. *J Immunol* (2011) 186(2):1032-43. doi: 10.4049/jimmunol.1001893. PubMed PMID: 21149601; PubMed Central PMCID: PMCPMC3178067.

37. de Bruin AM, Libregts SF, Valkhof M, Boon L, Touw IP, Nolte MA. IFNgamma induces monopoiesis and inhibits neutrophil development during inflammation. *Blood* (2012) 119(6):1543-54. doi: 10.1182/blood-2011-07-367706. PubMed PMID: 22117048.

38. Cunningham CR, Champhekar A, Tullius MV, Dillon BJ, Zhen A, de la

Fuente JR, et al. Type I and Type II Interferon Coordinately Regulate Suppressive Dendritic Cell Fate and Function during Viral Persistence. *PLoS Pathog* (2016) 12(1):e1005356. doi: 10.1371/journal.ppat.1005356. PubMed PMID: 26808628; PubMed Central PMCID: PMCPMC4726812.

39. Moskophidis D, Battegay M, Bruendler MA, Laine E, Gresser I, Zinkernagel RM. Resistance of lymphocytic choriomeningitis virus to alpha/beta interferon and to gamma interferon. *Journal of Virology* (1994) 68(3):1951-5.

40. Helft J, Bottcher J, Chakravarty P, Zelenay S, Huotari J, Schraml BU, et al. GM-CSF Mouse Bone Marrow Cultures Comprise a Heterogeneous Population of CD11c(+)MHCII(+) Macrophages and Dendritic Cells. *Immunity* (2015) 42(6):1197-211. doi: 10.1016/j.immuni.2015.05.018. PubMed PMID: 26084029.

41. Kalia V, Sarkar S, Subramaniam S, Haining WN, Smith KA, Ahmed R. Prolonged interleukin-2Ralpha expression on virus-specific CD8+ T cells favors terminal-effector differentiation in vivo. *Immunity* (2010) 32(1):91-103. doi: 10.1016/j.immuni.2009.11.010. PubMed PMID: 20096608.

42. Arsenio J, Kakaradov B, Metz PJ, Kim SH, Yeo GW, Chang JT. Early specification of CD8+ T lymphocyte fates during adaptive immunity revealed by single-cell gene-expression analyses. *Nat Immunol* (2014) 15(4):365-72. doi:

10.1038/ni.2842. PubMed PMID: 24584088; PubMed Central PMCID: PMCPMC3968536.

43. Kaech SM, Cui W. Transcriptional control of effector and memory CD8+ T cell differentiation. *Nat Rev Immunol* (2012) 12(11):749-61. doi: 10.1038/nri3307. PubMed PMID: 23080391; PubMed Central PMCID: PMCPMC4137483.

44. Manjunath N, Shankar P, Wan J, Weninger W, Crowley MA, Hieshima K, et al. Effector differentiation is not prerequisite for generation of memory cytotoxic T lymphocytes. *J Clin Invest* (2001) 108(6):871-8. doi: 10.1172/JCI13296. PubMed PMID: 11560956; PubMed Central PMCID: PMCPMC200936.

45. Mueller K, Schweier O, Pircher H. Efficacy of IL-2- versus IL-15-stimulated CD8 T cells in adoptive immunotherapy. *Eur J Immunol* (2008) 38(10):2874-85. doi: 10.1002/eji.200838426. PubMed PMID: 18825743.

46. Belz GT, Heath WR, Carbone FR. The role of dendritic cell subsets in selection between tolerance and immunity. *Immunology & Cell Biology* (2002) 80(5):463-8. doi: doi:10.1046/j.1440-1711.2002.01116.x.

47. Whitmire JK, Tan JT, Whitton JL. Interferon-gamma acts directly on CD8+ T cells to increase their abundance during virus infection. *J Exp Med*

(2005) 201(7):1053-9. doi: 10.1084/jem.20041463. PubMed PMID: 15809350; PubMed Central PMCID: PMCPMC2213135.

48. Sercan O, Hammerling GJ, Arnold B, Schuler T. Cutting Edge: Innate Immune Cells Contribute to the IFN- -Dependent Regulation of Antigen-Specific CD8+ T Cell Homeostasis. *The Journal of Immunology* (2006) 176(2):735-9. doi: 10.4049/jimmunol.176.2.735.

49. Sercan O, Stoycheva D, Hammerling GJ, Arnold B, Schuler T. IFN-gamma receptor signaling regulates memory CD8+ T cell differentiation. *J Immunol* (2010) 184(6):2855-62. doi: 10.4049/jimmunol.0902708. PubMed PMID: 20164422.

50. Wherry EJ, Ahmed R. Memory CD8 T-cell differentiation during viral infection. *J Virol* (2004) 78(11):5535-45. doi: 10.1128/JVI.78.11.5535-5545.2004. PubMed PMID: 15140950; PubMed Central PMCID: PMCPMC415833.

51. Goldszmid RS, Caspar P, Rivollier A, White S, Dzutsev A, Hieny S, et al. NK cell-derived interferon-gamma orchestrates cellular dynamics and the differentiation of monocytes into dendritic cells at the site of infection. *Immunity* (2012) 36(6):1047-59. doi: 10.1016/j.immuni.2012.03.026. PubMed PMID: 22749354; PubMed Central PMCID: PMCPMC3412151.

52. de Bruin AM, Buitenhuis M, van der Sluijs KF, van Gisbergen KP, Boon

L, Nolte MA. Eosinophil differentiation in the bone marrow is inhibited by T cell-derived IFN-gamma. *Blood* (2010) 116(14):2559-69. doi: 10.1182/blood-2009-12-261339. PubMed PMID: 20587787.

53. Kalia V, Sarkar S. Regulation of Effector and Memory CD8 T Cell Differentiation by IL-2-A Balancing Act. *Front Immunol* (2018) 9:2987. doi: 10.3389/fimmu.2018.02987. PubMed PMID: 30619342; PubMed Central PMCID: PMCPMC6306427.

54. Pipkin ME, Sacks JA, Cruz-Guilloty F, Lichtenheld MG, Bevan MJ, Rao A. Interleukin-2 and inflammation induce distinct transcriptional programs that promote the differentiation of effector cytolytic T cells. *Immunity* (2010) 32(1):79-90. doi: 10.1016/j.immuni.2009.11.012. PubMed PMID: 20096607; PubMed Central PMCID: PMCPMC2906224.

55. Granucci F, Vizzardelli C, Pavelka N, Feau S, Persico M, Virzi E, et al. Inducible IL-2 production by dendritic cells revealed by global gene expression analysis. *Nature Immunology* (2001) 2:882. doi: 10.1038/ni0901-882.

56. Boyman O, Sprent J. The role of interleukin-2 during homeostasis and activation of the immune system. *Nat Rev Immunol* (2012) 12(3):180-90. doi: 10.1038/nri3156. PubMed PMID: 22343569.

57. Granucci F, Feau S, Angeli V, Trottein F, Ricciardi-Castagnoli P. Early

IL-2 production by mouse dendritic cells is the result of microbial-induced priming. *J Immunol* (2003) 170(10):5075-81. doi: 10.4049/jimmunol.170.10.5075. PubMed PMID: 12734352.

58. Surh CD, Sprent J. Homeostasis of naive and memory T cells. *Immunity* (2008) 29(6):848-62. doi: 10.1016/j.immuni.2008.11.002. PubMed PMID: 19100699.

59. Becker TC, Wherry EJ, Boone D, Murali-Krishna K, Antia R, Ma A, et al. Interleukin 15 is required for proliferative renewal of virus-specific memory CD8 T cells. *J Exp Med* (2002) 195(12):1541-8. doi: 10.1084/jem.20020369. PubMed PMID: 12070282; PubMed Central PMCID: PMCPMC2193552.

60. Zhang X, Sun S, Hwang I, Tough DF, Sprent J. Potent and Selective Stimulation of Memory-Phenotype CD8+ T Cells In Vivo by IL-15. *Immunity* (1998) 8(5):591-9. doi: https://doi.org/10.1016/S1074-7613(00)80564-6.

61. Dubois S, Mariner J, Waldmann TA, Tagaya Y. IL-15Rα Recycles and Presents IL-15 In trans to Neighboring Cells. *Immunity* (2002) 17(5):537-47. doi: https://doi.org/10.1016/S1074-7613(02)00429-6.

62. Chang JT, Palanivel VR, Kinjyo I, Schambach F, Intlekofer AM, Banerjee A, et al. Asymmetric T Lymphocyte Division in the Initiation of Adaptive Immune Responses. *Science* (2007) 315(5819):1687-91. doi:

10.1126/science.1139393.

63. King CG, Koehli S, Hausmann B, Schmaler M, Zehn D, Palmer E. T cell affinity regulates asymmetric division, effector cell differentiation, and tissue pathology. *Immunity* (2012) 37(4):709-20. doi: 10.1016/j.immuni.2012.06.021. PubMed PMID: 23084359; PubMed Central PMCID: PMCPMC3622938.

64. Hey YY, Quah B, O'Neill HC. Antigen presenting capacity of murine splenic myeloid cells. *BMC Immunol* (2017) 18(1):4. doi: 10.1186/s12865-016-0186-4. PubMed PMID: 28077081; PubMed Central PMCID: PMCPMC5225582.

65. Tacke F, Ginhoux F, Jakubzick C, van Rooijen N, Merad M, Randolph GJ. Immature monocytes acquire antigens from other cells in the bone marrow and present them to T cells after maturing in the periphery. *J Exp Med* (2006) 203(3):583-97. doi: 10.1084/jem.20052119. PubMed PMID: 16492803; PubMed Central PMCID: PMCPMC2118235.

66. Larson SR, Atif SM, Gibbings SL, Thomas SM, Prabagar MG, Danhorn T, et al. Ly6C(+) monocyte efferocytosis and cross-presentation of cell-associated antigens. *Cell Death Differ* (2016) 23(6):997-1003. doi: 10.1038/cdd.2016.24. PubMed PMID: 26990659; PubMed Central PMCID: PMCPMC4987733.

국문 초록

단구-유래 항원 제시 세포 (Monocyte-derived dendritic cell; moDC)는 평상시에는 드물게 존재하지만, 각종 감염 및 염증 환경에서 그 수가 폭발적으로 증가한다고 알려져 있다. 하지만, moDC의 정확한 분화 기전이나 CD8 T 세포의 기능에 미치는 영향 등은 아직 불분명한 부분이 많다. 본 연구에서는 moDC의 분화 과정과 이 세포가 CD8 T 세포 반응에 어떤 역할을 하는지를 규명하였다. 먼저 급성 *Lymphocytic Choriomeningitis virus* (LCMV) 로 감염한 마우스 체내 장기 및 혈액에 moDC가 감염이 진행될수록 그 수가 증가하는 것을 관찰하였고, 염증성 사이토카인 IFN-γ를 중화하였을 때 moDC의 수가 감소하는 것을 확인함으로써 moDC의 증가가 IFN-γ 의존적인 현상임을 규명하였다. 또한, 골수의 전구세포 중 common monocyte progenitor cells (cMoPs)가 IFN-γ의 수용체를 특징적으로 높게 발현하고 있음을 보여주었고, 이 전구 세포가 IFN-γ의 신호를 직접 받아 moDC로 분화하는 세포임을 확인하였다.

moDC 또는 기존 CD8 T 세포를 자극하여 활성화시킨다고 알려진 수지상 세포 (conventional dendritic cell; cDC)를 시험관 내에서 CD8 T 세포와 함께 배양하고 CD8 T 세포의 분화 양상을 관찰했을

때, 두 종류의 항원 제시 세포가 CD8 T 세포 분화를 다르게 조절하는 것을 확인할 수 있었다. cDC에 의해 자극된 CD8 T 세포가 효과적으로 항원-특이적인 세포 사멸능을 가지는 데에 반해, moDC의 자극을 받은 CD8 T 세포는 그 능력이 감소되어 있었다. 하지만, moDC에 의해 자극된 CD8 T 세포는 더 오래 살아남는 기억 세포로 분화하는 양상을 나타내었다. moDC가 결핍되어 있는 마우스에 LCMV를 감염시켰을 때에도, 해당 마우스는 효과기 T 세포 반응을 유지하고 있는 반면에 기억 T 세포 반응은 현저히 저하되어 있었다. moDC는 cDC보다 T 세포 활성화에 중요한 사이토카인인 IL-2를 생성하는 능력이 낮았고, 이것이 moDC가 CD8 T 세포를 기억 세포로 분화시키는 능력을 부여함을 확인하였다. 본 연구는 CD8 T 세포의 기억 세포로의 분화가 moDC의 자극을 받아 일어난다는 것을 규명함으로써, 백신 개발 전략에 새로운 타겟을 제시하였다는 데에 의의가 있다.

주요어: 감염성 질환, LCMV, 단구-유래 항원 제시 세포, IFN-γ, 세포성 면역, 수지상 세포, CD8 T 세포

학번: 2012-21595